Article:

Ramos, A, Gomes Correia, A, Calçada, R et al. (1 more author) (2022) Ballastless railway track transition zones: An embankment to tunnel analysis. Transportation Geotechnics, 33. 100728. ISSN 2214-3912

https://doi.org/10.1016/j.trgeo.2022.100728

Ballastless railway track transition zones: an embankment to tunnel analysis

Ramos, A[a*], Gomes Correia, A. [a], Calçada, R.[b], Connolly, D.P. [c]

[a*]*Ana Ramos, University of Minho, ISISE, Department of Civil Engineering, Portugal (ana.l.g.ramos@gmail.com) – corresponding author*

[a]*António Gomes Correia, University of Minho, ISISE, Department of Civil Engineering, Portugal (agc@civil.uminho.pt)*

[b]*Rui Calçada, CONSTRUCT – LESE, Faculty of Engineering, University of Porto, Portugal (ruiabc@fe.up.pt)*

[c]*David P Connolly, University of Leeds, Institute for High Speed Rail and System Integration, UK (d.connolly@leeds.ac.uk)*

Ballastless railway track transition zones: an embankment to tunnel analysis

Railway track transition zones are characterised by an abrupt change in track support stiffness, which increases dynamic wheel loads and leads to the acceleration of differential settlement and track degradation. The performance of transition zones is a concern for railway Infrastructure Managers due to the increased maintenance operations and costs typically associated with these short track sections. To date, the majority of transition zone studies are focused on the analysis of ballasted tracks, however, the popularity of ballastless track has been increasing, especially on high-speed lines. Therefore, this work aims to study concrete slab track transition zones, with a focus on embankment/plain line-to-tunnel sections. The analysis uses a hybrid methodology, combining 3D finite element modelling with empirical settlement equations, in an iterative manner. The finite element model is capable of simulating train-track interaction and uses contact elements to simulate the potential detachment (voiding) between the slab's hydraulically bound layer and frost protection layer. At each iteration, firstly the track-ground stress fields are calculated using a 3D model, before passing them to a calibrated empirical equation capable of computing settlement across the transition. Then, before starting the next iteration, these settlements are used to modify the 3D model geometry, thus account for the effects of the previous settlement, before computing the updated stress fields. The model is used to analyse settlement and stresses for a transition zone case-study, before study the ability of a resilient mat to improve the performance of the track.

Keywords: Ballastless track; Railway transition zone; Embankment-tunnel transition zone; Railway track settlement; Train-track railway dynamics

List of abbreviations, acronyms and symbols

FEM – Finite Element Method

LVDT – Linear Variable Differential Transformer

HBL – Hydraulically Bonded Layer

FPL – Frost Protection Layer

EPDM – Ethylene Propylene Diene Monomer

FKN – Normal penalty stiffness factor

k – stiffness

c – viscous damper

E – *Young* modulus

γ – dry density

ρ – mass density

ν – *Poisson*'s ratio

αi – parameter of the damping Rayleigh matrix that corresponds to the material i that multiplies the mass' matrix of the system

βi – parameter of the damping Rayleigh matrix that corresponds to the material *i* that multiplies the global stiffness's matrix (K_i))

ξ – hysteric damping

f – frequency

M_b – mass of the bogies

M_e – mass of the wheelset

K_p – stiffness of the primary suspension

c_p – damping of the primary suspension

K_h – contact stiffness

c – cohesion

ϕ – friction angle

μ – friction coefficient

p – mean stress

q – deviatoric stress

p_{am} – mean stress induced by the passage of the vehicle

q_{am} – deviator stress induced by the passage of the vehicle

m – slope of the line of the critical state in the referential p-q

s – ordinate of the line of the critical state in the referential p-q when p is null

N – number of load cycles

ΔN – set of cycles

p_{ini} – initial isotropic stress

q_{ini} – initial soil deviator stress

B, a and ε_l^{po} –material constants of the empirical model

δ – cumulative permanent displacement

1 Introduction

Transition zones are characterized by an abrupt change in the track stiffness and development of differential/asymmetric settlements leading to the growth of bumps and dips (Figure 1.1). These phenomena are the source of passenger discomfort, lack of circulation safety and an important cause of the increasing maintenance costs (Fröhling et al., 1996, Hunt, 1997, Nicks, 2009). This subject is of great interest from several points of view - structural, geotechnical and economical – and a concern for railway Infrastructure Managers.

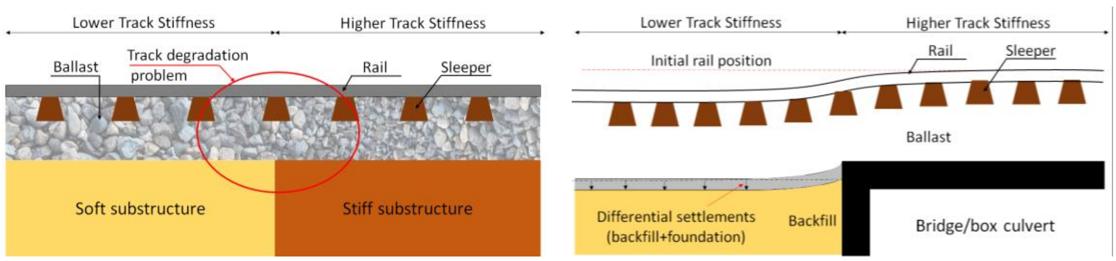

a) b)

Figure 1.1 – a) Schematic representation of the abrupt variation in track stiffness - based on Paixão et al. (2013); b) differential settlement of the backfill and its foundation (based on Paixão et al. (2013))

The track degradation phenomenon in a transition zone starts with the abrupt changes in support stiffness, increasing the dynamic wheel load and the rate at which the track geometry degrades (Dahlberg, 2004, Zhang et al., 2007, Ferreira and López-Pita, 2013, Asghari et al., 2021). This change in the displacements will excite the train components (namely the wheels, bogies and car body of the vehicles), which will have an impact on the dynamic amplification of the vertical train-track interaction forces. This degradation is the cause of the generation of noise, vibration, poor ride comfort, and higher risks of derailment (Paixão et al., 2016). Indeed, these problems can lead to the appearance of hanging sleepers, permanent rail deformations, ballast penetration into the subgrade, cracking of concrete sleepers and/or concrete slab, and loss of gauge (Banimahd et al., 2012). Indeed, there is an inter-dependency of enhanced dynamic loads and differential settlement, and their relationship to track degradation (Indraratna et al., 2019, Paixão, 2014). This degradation process is a self-perpetuating cycle since settlements can lead to the amplification of dynamic loads, which leads to an increase in the differential settlement (Banimahd et al., 2012).

Track transitions can occur in several situations: ballasted track underlain by a natural ground and the track underlain by a hard structure such as a bridge, tunnel, or culvert (Hunt, 1997, Fröhling et al., 1996, AREMA, 2005, Lundqvist et al., 2006, Coelho et al., 2011) or even in the case of a conventional track that changes to ballastless track to cross a roadway, a waterway (canal, river, etc.) or valleys through bridges or level crossings (Indraratna et al., 2019).

Due to the increasing popularity of ballastless tracks, the number of areas where there is a transition between ballasted and ballastless tracks is also increasing. Some examples of transition zones are depicted in Figure 1.2. Thus, solutions are required to mitigate the impact caused by the structural discontinuities along the track (Varandas et al., 2013). These aim to minimise any abrupt variations in track stiffness and ensure a smooth and gradual change from a less stiff (ballasted track) to a more stiff (ballastless track) structure (Indraratna et al., 2019). One of the main goals consists in choosing an efficient approach and the most suitable construction method (Shahraki and Witt, 2015).

a)

b)

c) d)

Figure 1.2 – Examples of transition zones (Alves Ribeiro, 2012): a) transition embankment-bridge; b) inferior crossing to the track; C) transition to a tunnel; d) transition between a ballasted and slab tracks on the high-speed line Cordoba- Malaga (Spain) (Sañudo et al., 2016)

This work aims to analyse the performance of a specific transition zone, where although the track is solely ballastless, the support changes from an embankment to a tunnel with higher stiffness.

Over the years, ballastless track has proven attractive and extensively used on high-speed lines. This because it can potentially offer improved long-term performance and lower permanent deformation. However, the effect of transitioning support stiffness's across slab track is still largely unexplored, with much of previous research based on the transitions between ballasted and ballastless tracks (Li and Wu (2008), Shahraki and Witt (2015), Shahraki et al. (2015) and Wang and Markine (2019)), or between ballasted tracks and a stiff structure as a bridge or box culvert (Coelho et al. (2011), Varandas et al. (2011), Varandas et al. (2013), Alves Ribeiro et al. (2015), Paixão et al. (2016), Momoya et al. (2016), Varandas et al. (2016), Wang and Markine (2018), Alves Ribeiro et al. (2018) and Li et al. (2021)). Alternatively, Yu et al. (2019) studied the effect of a subgrade transition, however for an asphalt-ballast slab track. The high number of works focused on ballasted track is understandable because it is widely used, particularly for non-high speed lines. Moreover, ballasted track is potentially subject to higher permanent deformations when compared to the slab track, which means that it is often studied with respect to long-term performance. Thus, it expected that at transition zones, ballastless track can offer better long-term performance compared to ballasted track. However, the deformation tolerances of ballastless track in terms of differential settlement are reduced compared to the ballasted track, due to the high cost of maintenance. This means that the long-term performance of ballastless tracks (especially in transition zones) demands extra attention in order to avoid cracks in the concrete, and high levels of differential settlement.

One work that has been performed on the subject, was the analysis of transitions across ballastless tracks by Shan et al. (2013). In this work, the authors considered a moving point load, thus ignoring vehicle-track dynamic interaction, which can play an important role. Therefore, in this analysis, the short and long term behaviour of ballastless track at a transition zone is analysed through the evaluation of the displacements and stresses, accounting for the interaction forces between vehicle and track. The long-term analysis is performed through an innovative hybrid methodology based on the implementation of a calibrated (Ramos, 2021) empirical permanent deformation model which allows simulation of the development of the permanent deformations based on the stress levels. The calibration process developed previously (and respective methodology) is vital in the prediction of the long-term behavior of track structures, especially for ballastless transition zones. Thus, the development of numerical studies with the implementation of calibrated properties can be an important tool in the scope of the study of the long-term performance of ballastless transition zones. The approach uses 3D FEM (finite element method) modelling developed in ANSYS, where the detachment between the superstructure and substructure is simulated using contact elements. The permanent deformations are processed in MATLAB before imposing on the FEM model to simulate the degradation of the track.

2 Description of the case study

This analysis aims to study the amplification dynamic effects generated by the passage of the *Alfa-Pendular* train (Figure 2.1) considering a stiffness difference between two structures with different supports: a ballastless track over an embankment and a ballastless track in a tunnel. Figure 2.2 a) shows an overview of this situation. In this problem, the tunnel presents a much higher stiffness when compared to the ballastless track supported by an embankment. The general effects of this stiffness' difference are depicted in Figure 2.2 b) (schematic representation).

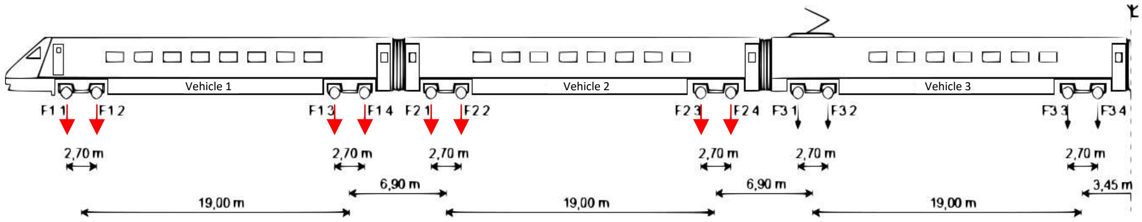

Figure 2.1 – Geometry of the *Alfa Pendular* train (showing the first four cars only)

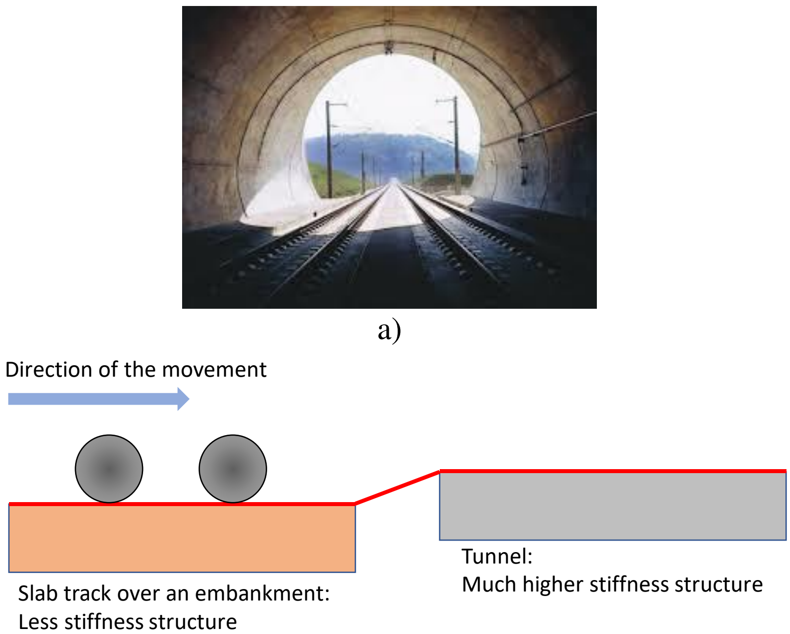

a)

b)

Figure 2.2 - Example of the transition: slab track in a tunnel (a) and its effect due to the stiffness's difference

2.1 *Finite elements model*

2.1.1 Material properties

The ballastless track is composed of rails, railpads, concrete slab, HBL (hydraulically bonded layer) and a substructure that includes the FPL (frost protection layer) and subgrade. The section placed on the embankment is depicted in Figure 2.3.

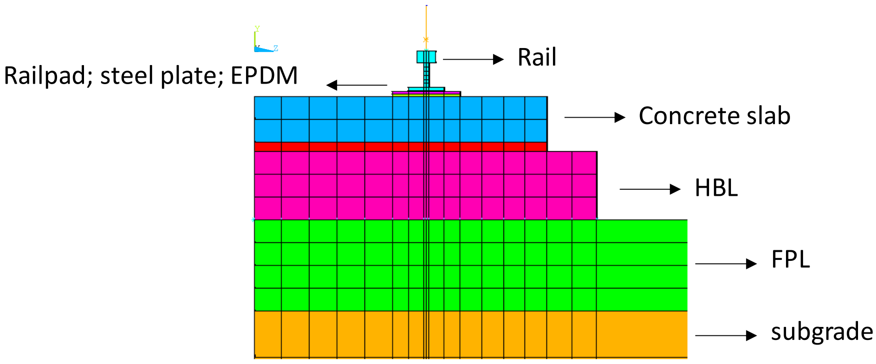

Figure 2.3 - Materials that composed the ballastless track

The adopted material parameters are based on a previous calibration study (Ramos et al., 2021) and are depicted in Table 2.1. This calibration is based on experimental results obtained in a physical model of a ballastless track 2.2 m long, subject to more than 3 million load cycles. The adjustment of the materials' properties (in terms of *Young* modulus and *Poisson's* ratio) of the ballast, FPL, subgrade and railpad was performed through the comparison between the numerical and experimental displacements from the LVDTs placed on the track. The obtained calibrated properties are within with the values described in the bibliography.

Table 2.1 - Ballastless track properties

Material	**Properties**
Rail (BS113A)	$E=200\times10^9$ Pa $\gamma=7850$ kg/m^3 $\nu=0.30$

Railpad	k=1800×10^6 N/m γ=1000 kg/m^3 ν=0.30 E=k×thickness/area
Steel Plate	E=210×10^9 Pa γ=7850 kg/m^3 ν=0.30
EPDM – ethylene propylene diene monomer	k=40×10^6 N/m γ=1200 kg/m^3 ν=0.00 E=k×thickness/area
Cement grout mass	E=25×10^9 Pa γ=2000 kg/m^3 ν=0.25
Concrete Slab	E=40×10^9 Pa γ=2500 kg/m^3 ν=0.25
HBL	E=15×10^9 Pa γ=2400 kg/m^3 ν=0.25
FPL	E=3.3×EV_2=3.3×135×10^6 Pa γ=2141 kg/m^3 ν=0.35
Subgrade	E=3.3×EV_2=3.3×65×10^6 Pa γ=2091 kg/m^3 ν=0.35

E = *Young* modulus; *γ* = density; *ν* = *Poisson*'s ratio; *k*=stiffness

The damping values were determined based on the *Rayleigh* damping matrix. The αi (parameter of the Rayleigh damping matrix that corresponds to the material *i* that multiplies the mass' matrix of the system) and βi (parameter of the Rayleigh damping matrix that corresponds to the material *i* that multiplies the global stiffness's matrix (K_i))

values were estimated based on numerical receptance curves obtained from the excitation of the rail in two sections of the track with different characteristics: over the embankment and over the tunnel. A Dirac impulse was applied on the numerical model of the track and for all materials, $\xi_1 = \xi_2$ was assumed. In the case of the concrete materials and geomaterials, a hysteretic damping of $\xi=0.01$ and $\xi=0.03$ was adopted, respectively. Regarding the railpads (EPDM) since these elements are modelled by solid finite elements and not by spring-damper elements, hysteretic damping was adopted (equal to $\xi=0.05$), instead of the definition of the stiffness (k) and viscous damper (c). The obtained receptance curves, which allow the identification of the resonances of the structure by measuring the transfer from force on rail to associated displacement, are depicted in Figure 2.4. This figure shows that the receptance curve of the rail in the embankment and the tunnel are similar since the response of the rail is highly influenced by the properties of the railpads, which are the same in both analyses. The main difference occurs at the concrete slab level (Figure 2.4 b). The results show the values of the receptance peaks are lower in the ballastless track over the tunnel as expected due to the lower stiffness of the structure. Thus, according to these results, a range of frequencies between 5 Hz (f_1) and 200 Hz (f_2) was adopted. This range is considered enough to correctly represent the response of the track. From these assumptions, the parameters α and β of each material are presented in Table 2.2.

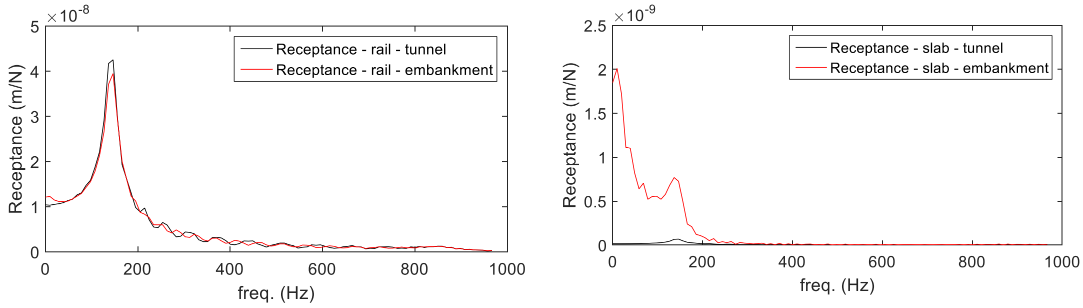

a) b)

Figure 2.4 – Receptance curves: a) of the rail (top); b) of the concrete slab (top)

Table 2.2 – Damping Rayleigh parameters

Material	ξ	α (s^{-1})	β (s)
Railpad - EPDM	0.05	5.712	0.00014
Concrete slab and HBL	0.01	1.142	2.894E-05
Substructure (FPL and subgrade)	0.03	3.427	8.681E-05

ξ=hysteretic damping; α= parameter of the damping Rayleigh matrix that multiplies the mass' matrix of the system; β=parameter of the damping Rayleigh matrix that multiplies the global stiffness's matrix

2.1.2 Geometry and characteristics

The 3D model is depicted in Figure 2.5 and presents a total length of 53.1 m (the embankment with 31.65 m and the tunnel with 21.45 m). The analysis was performed considering the passage of an *Alfa Pendular* train running at a speed equal to 220 km/h.

Regarding the boundaries, viscous dampers (Lysmer and Kuhlemeyer, 1969) were used to attenuate the waves that impinge the vertical boundaries of the FPL and subgrade layers. This approach has been used in the scope of the 3D modelling and transition zones with good results (Banimahd et al., 2012, Connolly et al., 2013, Woodward et al., 2015, Varandas et al., 2016, Shahraki and Witt, 2015, Alves Ribeiro et al., 2018). The wave propagation is due to the mobile character of the loading that simulates the passage of the train. Thus, at the bottom of the soil layer (horizontal boundary defined by the plane *xz with* y=-11.538 m), fixed supports were implemented. Regarding the part of the slab track in the tunnel, fixed supports in the vertical direction were also used at the bottom of the HBL layer. Since this is a large domain, symmetric conditions were adopted to reduce the computational effort. The support conditions of the model depicted in Figure 2.5 are explained and described in Table 2.3.

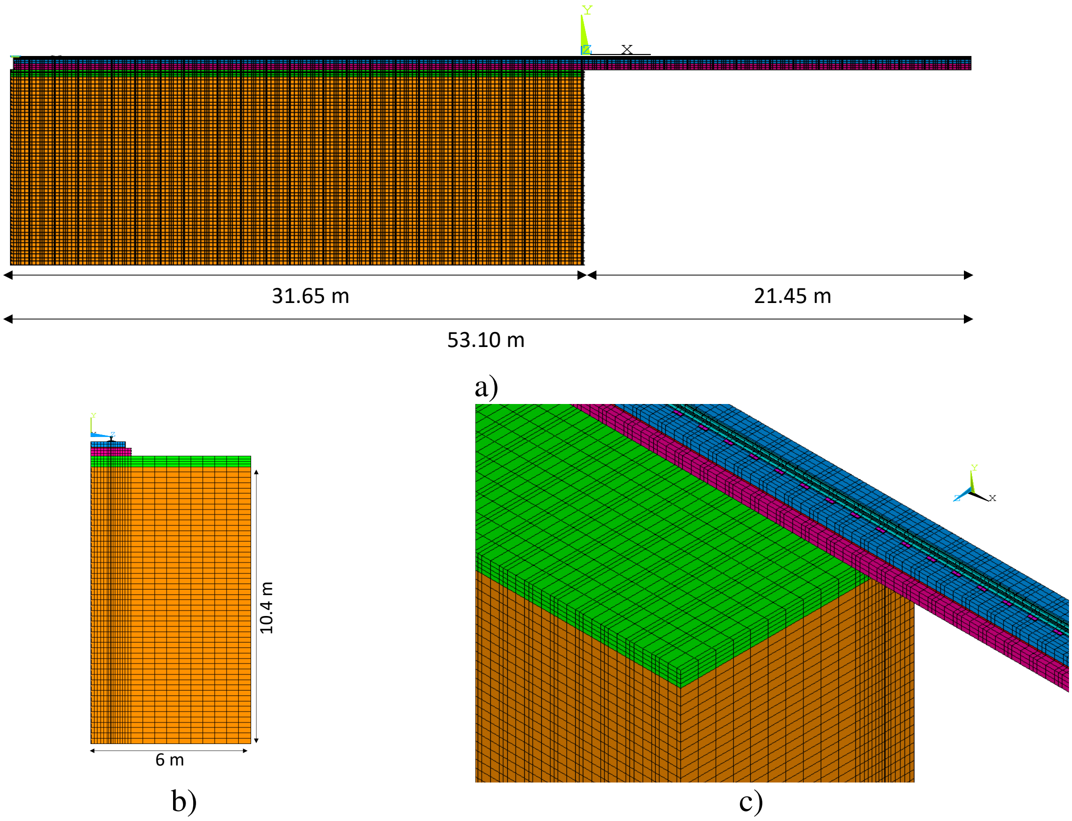

Figure 2.5 - Dimensions of the transition model: a) longitudinal section; b) cross-section; c) detail of the transition

Table 2.3 - Support conditions

Bottom of the model (plane *xz;* y=-11.538 m) – embankment	Fixed supports (all)
Bottom of the model (plane *xz;* y=-0.738) - tunnel	Fixed supports in the y-direction (vertical direction).
Plane *yx* (z=0) - plane of symmetry	Fixed supports in the *z*-direction (transversal direction)
Plane *yz* (x=0m) – located in the transition	Fixed supports in the *x*-direction (longitudinal direction) applied on FPL and subgrade
Plane *yz* (x=-31.65m)	Viscous dampers (all directions) applied on the FPL and subgrade
Plan *yx* (z=6.0m)	Viscous dampers (all directions) applied on the FPL and subgrade

The materials were modelled with solid elements (8 nodes). Contact elements were used to simulate the interaction between the vehicle and the track (through the implementation of *Hertzian* theory) and also to simulate the interaction between the support layer (HBL - superstructure) and the FPL, which is part of the substructure. These contact elements were used to simulate the “detachment” between both elements (HBL and FPL) during and after the passage of the train. This attempts to replicate the real behaviour of the railway structures in transition zones, however, the implementation is not straightforward.

Firstly, it is necessary to include the gravity effect on the contact elements. Otherwise, there is an uplift of the rail and concrete slab in sections located before the transition zone, which does not correspond to the real behaviour of the structure. Furthermore, it is important to highlight that the *Normal penalty stiffness factor* (FKN) must not be so large otherwise it can lead to numerical instability. Indeed, a simulation with a higher value was considered, but the solution did not converge. In this case, a *Normal penalty stiffness factor* equal to 1×10^1 was used to simulate the interaction between the FPL and HBL. Previous studies (Alves Ribeiro, 2012, Paixão, 2014) used a similar value in the simulation contact problems of the ballasted track (sleeper-ballast contact). Alternatively, to simulate the train-track interaction, a *Normal penalty stiffness factor* equal to 1×10^4 was adopted.

The modelling considers the symmetric conditions, and the mesh was optimized in order to reduce the time of calculus. The dynamic analysis was performed using Newmark-Raphson method with a time step of 0.002 s.

3 Train-track dynamics

3.1 Modelling of the Alfa Pendular train

Bogies, primary suspension, mass and axle of the wheelset and *Hertzian* stiffness were used to simulate the interaction between the vehicle and the track. The bogies were modelled with very stiff beams with distributed mass (M_b) and the primary suspensions were modelled through a set of spring-damper (K_p and c_p) elements. The wheelset was modelled as a concentrated mass (M_e) and a spring with a stiffness defined using *Hertzian* theory (Johnson, 1985). The simplified modelling of the vehicle, despite some apparent limitation (it is expected that the pitch motion of the vehicle can change the vertical forces of the wheel-rail contact), in a dynamic analysis, where the excitation frequencies are framed in the mean range of frequencies, is normally enough (Nielsen et al., 2003).

The train was modelled with finite elements. The modelling is depicted in Figure 3.1 and the properties are presented in Table 3.1. Since only half of the track is modelled, the properties were divided by two. It is important to refer that the properties of the *Alfa Pendular* train are not the same along the train (namely the axle load) but, the differences are very small, so a constant value for each property was adopted to simplify the analysis.

Regarding the loading, a load of 67.5 kN was adopted to simulate the wheel load (half an axle load). Since the interaction between the train and the track was considered and taking into account that this train has a total length of 158.90 m, the simulation of the complete passage of the train would imply the adoption of a model four times longer. In order to minimise the run time, the simulation of the passage of the bogies was performed considering the following process: at the beginning of the analysis, all bogies are stationary, weightless and located at the same position, near one end of the model. In the subsequent time steps, axle loads, and motion attributes are assigned to each bogie, one by one, according to the train speed and axle configuration. As each bogie reaches the other end of the model, they are stopped, one by one, and the respective axle loads are removed. This means that to each set of axles of a bogie, an evolution law of load over time is applied as well as an evolution law of movement (speed) over time. Thus, it is possible to simulate the passage of the different bogies of the train over a more reduced model. The increase in the calculation time is only a function of the time that the train takes to travel the model.

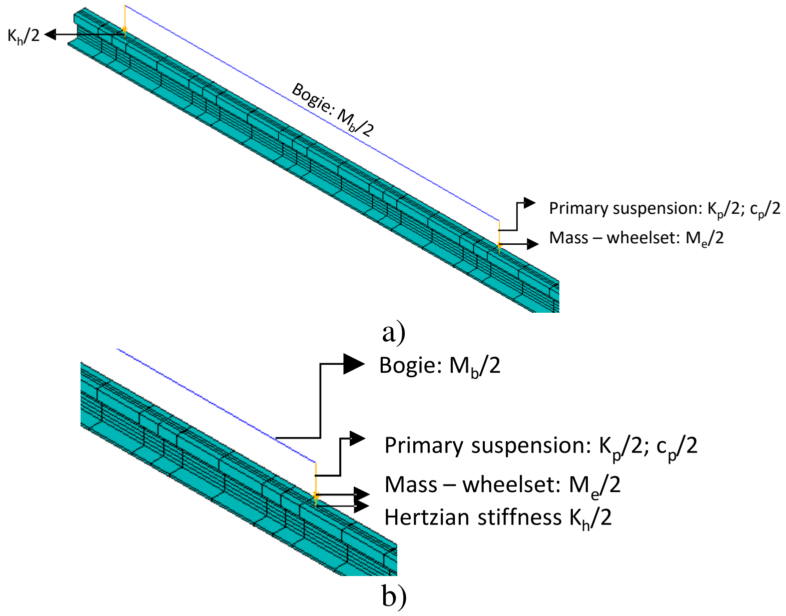

Figure 3.1 - Finite elements model (rail and the simplified model of the vehicle with the bogie, primary suspension, and mass of the wheel set): a) general view; b) detail of the modelling of the vehicle

Table 3.1 - Characteristics of the *Alfa Pendular* train adopted in this study

Component		Values
Bogie: $M_b/2$		4932/(2*2.7) [kg]
Primary suspension:	$K_p/2$	Primary suspension:
	$c_p/2$	36E3/2
Wheelset Mass: $M_e/2$		1800 (/2) [kg]
K_h		2.4×10^9 (/2) [N/m]

3.1.1 *Passage of the first 4 bogies*

In order to simulate the degradation process of the ballastless track in the transition zone, the effects of the passage of the first 4 bogies of the *Alfa Pendular* were analysed. This was chosen because from the 4th bogie, there is a repetition of the geometry of the train (Figure 2.1). The passage of the 4 bogies allows for the simulation of the effects of dynamic vehicle loads on the stress path and stress levels, which are important variables in the evolution of the permanent deformation.

In Figure 3.2, the load and speed functions (respectively) related to the passage of the first four bogies considering a train's speed of 220 km/h are presented. Analysing Figure 3.2, each bogie was loaded and animated with movement during a certain period, which corresponds to the time it takes to travel the entire model. For example, bogie 1 (black curve) loads the track and moves from 0 s to 0.69 s and bogie 2 (red curve) from 0.31 to 1 s. For example, at 0.5 s, 3 bogies are loading the track. The fourth bogie (blue curve) starts at 0.74 s.

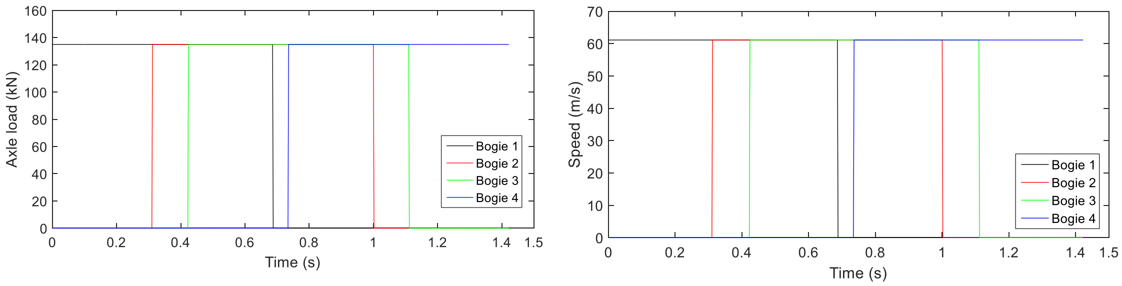

a) b)

Figure 3.2 – a) load function; b) speed function

Figure 3.3, Figure 3.4 and Figure 3.5 present the results regarding the displacements of the top nodes of the rail, concrete slab, FPL and subgrade and also the strains and stresses obtained on the top nodes of the subgrade. These results are obtained in the alignment under the loading area. The reference position corresponds to the transition zone at x=0 m. The instant t=0 s corresponds to the time the first bogie takes to reach the transition zone at x=0 m.

The results show that the maximum displacements/stresses/strains occur at the beginning of the loading during its application. However, this occurs far from the transition and these results were omitted to simplify the analysis of the performance of the ballastless track in this transition zone.

Analysing Figure 3.3, Figure 3.4 and Figure 3.5, the displacements, stresses and strains are stabilized until x=-5 m and they decrease as the train approaches the transition from the embankment to the tunnel. Regarding the concrete slab, FPL, and subgrade, the displacements in sections far from the transition are stabilised and are close to 0.55 mm. It is important to highlight that, in the case of rail displacements (Figure 3.3 a), it is possible to identify the passage of the axles of each bogie. However, the displacements of the concrete slab, FPL and subgrade (Figure 3.3 b, c and d) are not sensitive to the axles, but to the bogies. Regarding the stresses and strains at the top of the subgrade, the results show that, in sections far from the transition, the vertical stresses are close to 30 kPa and the vertical strains are close to 10×10^{-5}.

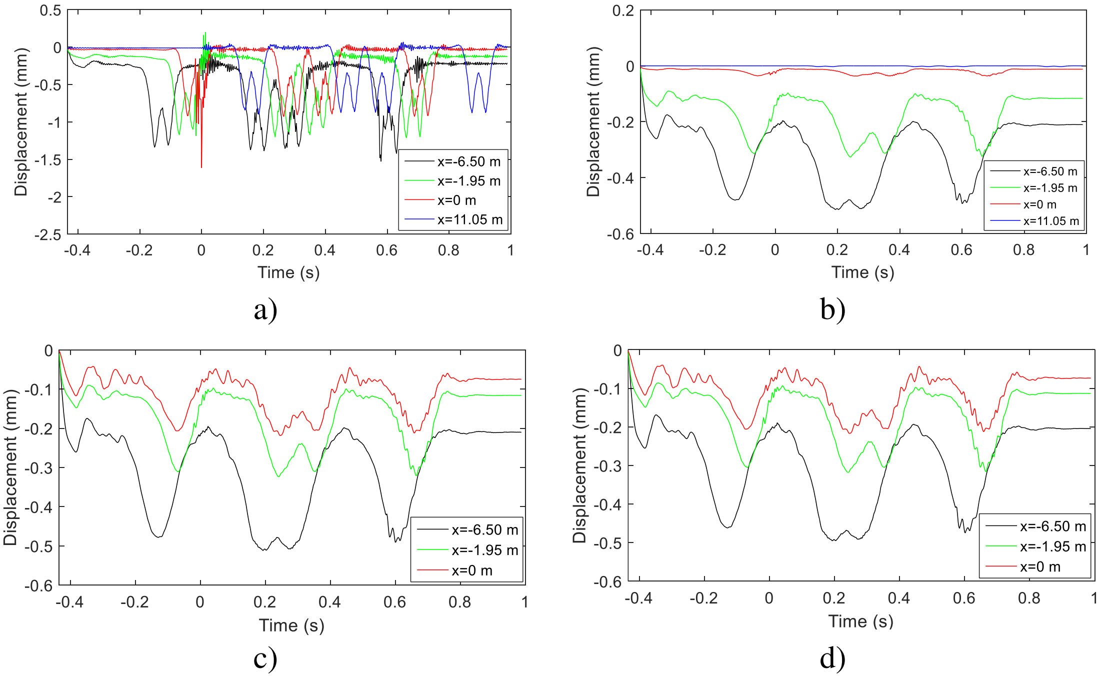

Figure 3.3 - Displacements of the top of the nodes of the: a) rails; b) concrete slab; c) FPL; d) subgrade

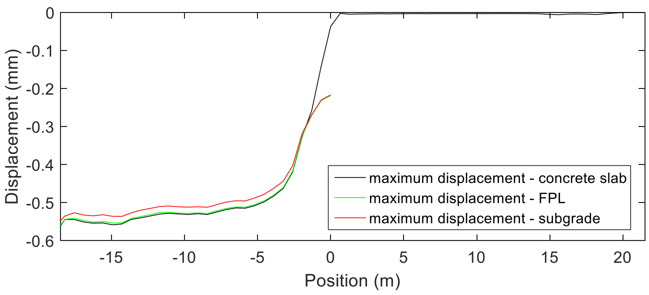

Figure 3.4 - Maximum displacement of the top nodes of the concrete slab, FPL and subgrade along the track

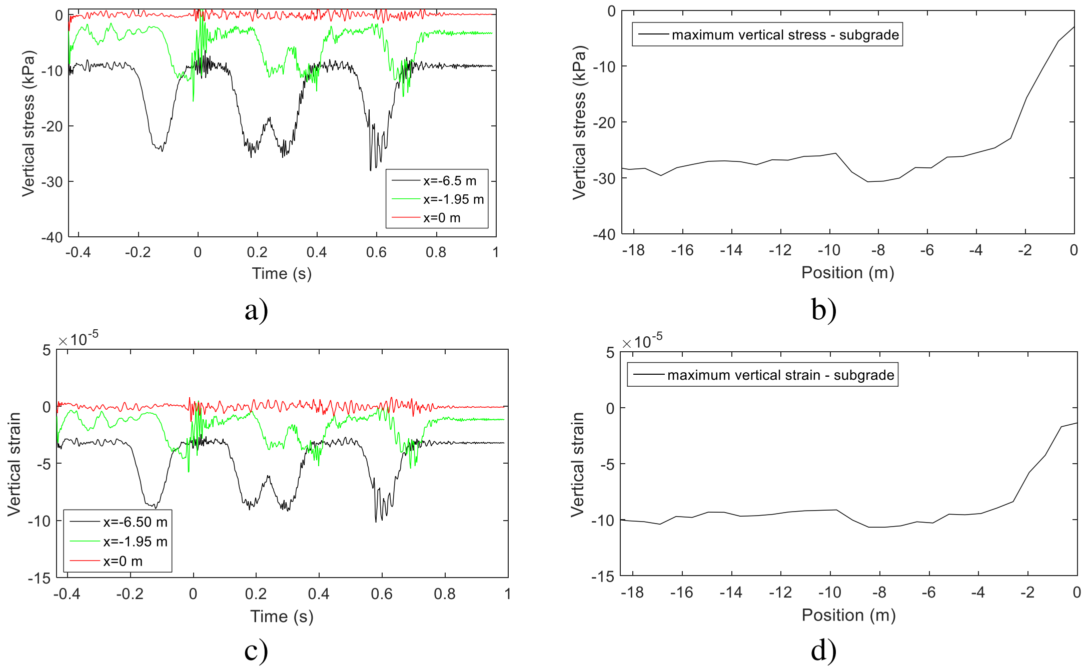

Figure 3.5 - Strain and stresses of the top nodes of the subgrade: a) subgrade's stress; b) maximum subgrade stress along the track; c) subgrade's strains; d) maximum subgrade strain along the track

3.1.1.1 Displacement of the wheel and interaction force vehicle-rail

The displacements, acceleration and interaction forces of axles of each bogie were determined and are depicted in Figure 3.6. The axles depicted in Figure 3.7 are representing each one of the bogies. The axles that belong to the same bogie present very similar results.

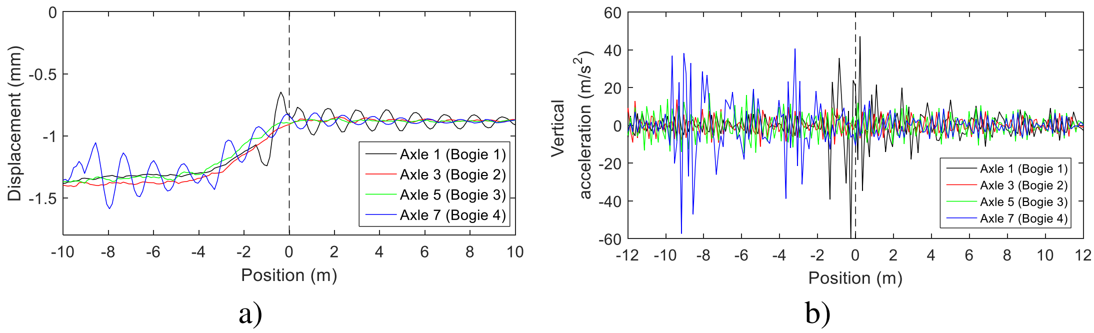

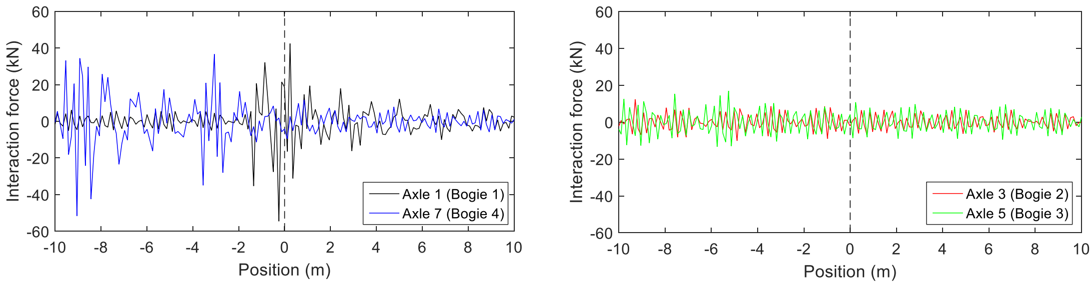

c) d)

Figure 3.6 - a) Vertical dynamic displacement of the axles; b) Variation of the vertical acceleration; c) Wheel-rail interaction forces (axle 1 and axle 7); d) Wheel-rail interaction forces (axle 3 and axle 5)

Analysing Figure 3.6, the dynamic displacement experienced by the wheel of the vehicle in the passage of the transition zone constitutes a measure of the variation of the stiffness of the track. As seen in Figure 3.6, the vertical displacement varies between 1.4 mm in the flexible zone and 0.85 mm in the stiffer zone (tunnel). The decrease of the displacements of all the axles corresponds to the passage of the transition zone. The vertical dashed line represented in Figure 3.6 identifies the transition between the embankment and the tunnel (x=0m).

The maximum acceleration of the axle of the vehicle is another control parameter in the dynamic response of the vehicle, which can also be adopted to verify the performance of the transition zones. In Figure 3.6 b), the variation of the vertical acceleration of the first, third, fifth, and seventh axles of the vehicle are represented. Some of the obtained values (axle 1 and axle 7) are above the alert limit, which is equal to 30 m/s^2, according to the limits established for the high-speed line Madrid-Seville (López-Pita et al., 2006). Axle 3 and axle 4 are far below the alert limit. The results show that there is an increment of acceleration's values of axle 1 during the passage of the transition zone. In the case of axle 7, this increment occurs slightly before the passage of the transition zone.

Figure 3.6 c) and d) presents the wheel-rail interaction force. Thus, from the vertical acceleration of the axle of the vehicle, it is possible to estimate the variation of the dynamic component of the interaction force wheel-rail, as depicted in Figure 3.6 c) and d). The dynamic component of the interaction force wheel-rail can be estimated by multiplying the vertical acceleration of the axle by the mass of the axle. The results regarding the first and also the seventh axles show an increment of the force during the transition zone, followed by a reduction of the force in the stiffer zone of the track.

3.1.1.2 Interaction forces HBL-FPL

The consideration of contact between the bottom of the HBL and the top of the FPL in the model allows for analysing the transmitted forces to the FPL and the identification of the "detachment" phenomenon, which is similar to the phenomenon of hanging sleepers. The consideration of the interaction between HBL-FPL in a model of finite elements implies the use of gravity at the beginning of the calculation before the passage of the vehicle. Furthermore, to simulate the contact between the HBL and FPL, a friction coefficient of 0.62 was adopted. This value was determined based on the following expression and considering a friction angle of the FPL equal to 48º:

$$\mu = tan\left(\frac{2}{3}\phi\right) \tag{3.1}$$

In Figure 3.7, the interaction forces between HBL-FPL (in the alignment under the rail) are represented. The nature of this contact is different from the wheel-rail contact and the results should be analysed in terms of contact stresses. However, the forces were extracted along the nodes (nodal forces) under the selected alignment. Thus, the results are presented in terms of forces and not stresses. The contact stresses can be obtained by multiplying the interaction forces by the area of influence. To simplify the extraction of the results, the analysis and the data processing, the results related to the interaction forces between HBL and FPL are presented by the interaction forces and both by stresses. The results show the transition in a section far from the transition zone (x=-6.50 m) and also the variation of the maximum interaction forces along the track.

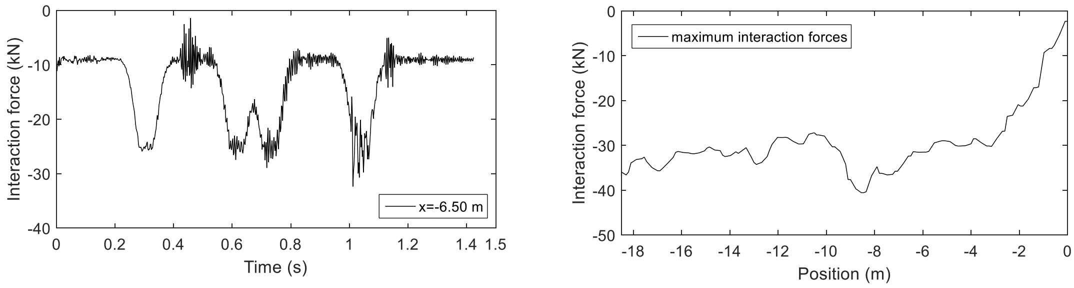

a) b)

Figure 3.7 – a) Interaction force HBL-FPL at x=-6.50 m; b) Maximum Interaction force HBL-FPL along the track

Analysing Figure 3.7, the interaction force varies over time between 0 kN and -40 kN (maximum value). The value of the interaction force is more or less stabilised in sections far from the transition zone (there are some oscillations, but they are not significant) and start to decrease as the train approaches the transition. Unfortunately, since the FPL is not modelled in the tunnel, it is not possible to analyse the interaction force along the transition force.

3.1.1.3 Track accelerations

In this section, the vertical accelerations of the concrete slab and HBL are presented. In Figure 3.8 a), the maximum and minimum values of the vertical acceleration in the top and bottom nodes of the concrete slab (under the loading alignment) along the transition zone are compared. Figure 3.8 b) presents the maximum and minimum values of the vertical acceleration in the top and bottom nodes of the HBL along the transition zone (also under the loading alignment).

The results show that the maximum values of vertical acceleration at the top nodes of the concrete slab are almost equal to the maximum values of the vertical acceleration at the bottom of the concrete slab. The same conclusions are obtained regarding the minimum vertical acceleration results. The results also show a decrease in the vertical acceleration on the transition. Regarding the HBL, the results show that the maximum values of the vertical accelerations at the top nodes of HBL are almost equal to the maximum values of the vertical accelerations at the bottom of this element. The same conclusions are obtained regarding the minimum vertical accelerations.

At the transition, there is a decrease in the vertical accelerations. The magnitude of the vertical accelerations on the concrete slab is similar to the vertical accelerations of the ballastless track presented in the work developed by Shan et al. (2013), where two different transition zones between a bridge and an ordinary subgrade are investigated using the finite element method. In this work, the vertical accelerations of the concrete slab vary between 3.5 m/s^2 and 6 m/s^2.

Furthermore, the vertical accelerations of the concrete slab along the transition zone are higher in the flexible zone when compared to the stiffer zone, and there is a slight increase immediately before the transition zone in the flexible zone in the concrete slab and HBL.

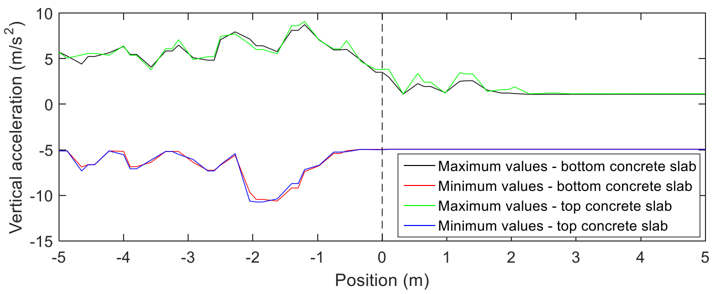

a)

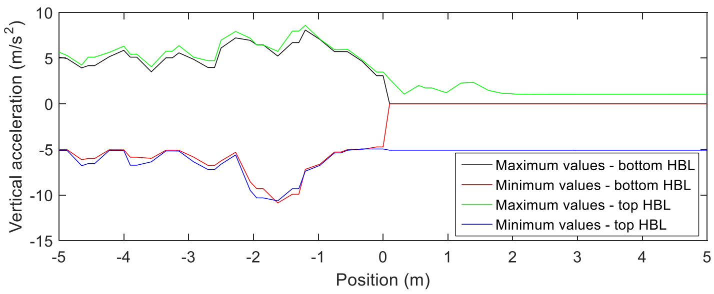

b)

Figure 3.8 - Maximum and minimum values of the vertical acceleration: a) of the concrete slab along the transition zone; b) of the HBL along the transition zone

3.1.1.4 Track stresses

After the analysis of the track accelerations, the stress results are presented and analysed in more detail. In Figure 3.9, the maximum and minimum values of the vertical and longitudinal stresses (tensile and compression) obtained along the transition zone at the top and bottom nodes of the concrete slab and HBL are presented. The points on the graph correspond to the nodal stresses of each finite element. These results are obtained for the nodes under the rail and the loading.

Regarding the concrete slab, it is possible to identify a peak in the transition zone in terms of longitudinal stresses (maximum values at the top of the layer). Analysing the vertical stresses, there is no clear peak in the transition zone, as in the longitudinal stresses. In the HBL, the analysis of results shows that in the transition zone, there is an increase of the vertical stresses (compression). The conclusions are similar regarding the longitudinal stresses. These layers (concrete slab and HBL) connect the embankment and the tunnel, ensuring the continuity of the track. Therefore, they experience a complex stress field aggravated due to the variation of the stiffness of the track in the transition. Furthermore, the results also show that, in the stiffer zone, the vertical stresses on the top nodes of HBL are slightly higher when compared to the flexible zone.

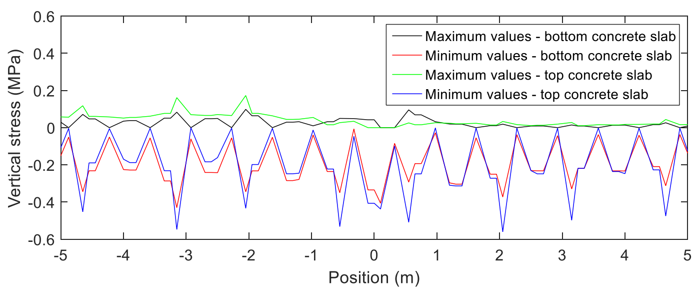

a)

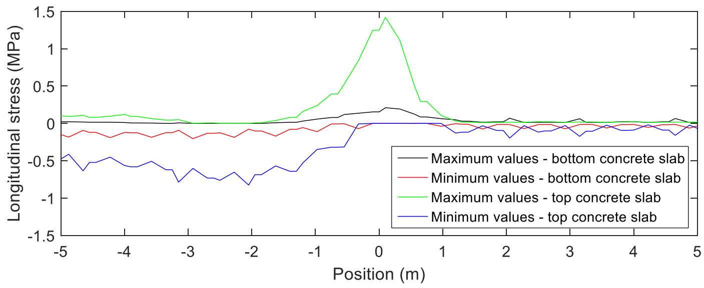

b)

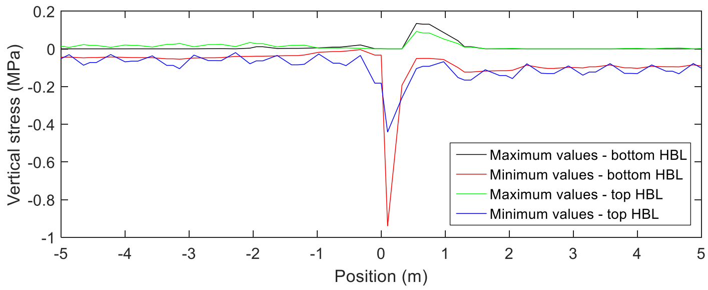

c)

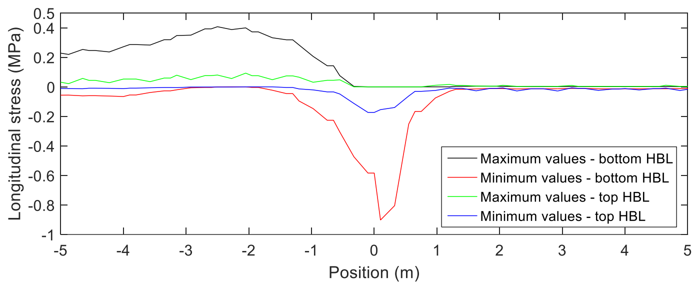

d)

Figure 3.9 – a) Vertical stresses in the top and bottom nodes of the concrete slab along the transition zone; b) longitudinal stresses in the top and bottom nodes of the concrete slab along the transition zone; c) vertical stresses in the top and bottom nodes of the HBL along the transition zone; d) longitudinal stresses in the top and bottom nodes of the HBL along the transition zone

3.2 Soil settlement simulation

The prediction of the settlement's evolution of the track implies knowledge about the long-term behaviour of the materials and the selection of models that can accurately simulate the dynamic behaviour of track. The incorporation of these results and deformation laws in complete models of the track is still a little explored field (Guo and Zhai, 2018) but some studies have been developed in this scope, as described in the work developed by Hunt (1996), Fröhling (1997), Abdelkrim et al. (2003), Ferreira (2010), Wang and Markine (2018) and more recently in Grossoni et al. (2021). The presented methodology to simulate the permanent deformation of the track is extremely versatile and can be adopted independently of the type of model or laws of permanent deformation. In this study, the evolution of the permanent deformation is only considered in the FPL and subgrade layers, applying the model developed by Chen et al. (2014). The parameters (material constants) were already calibrated and presented in the work developed by Ramos et al. (2021). The calibration was performed based on the comparison between the experimental and numerical cumulative permanent displacements. The calibrated empirical permanent deformation model was then applied to the extended ballastless track in the transition zone, in order to simulate its degradation process. The experimental results were obtained through the results of the LVDT's placed on some elements of the track of a physical ballastless track model (2.2 m long). The cyclic experimental tests were performed to simulate millions of cycles (3.4 million cycles) in just a few days of testing (Čebašek et al., 2018) , which facilitates the collection of a significant amount of data regarding the development of permanent deformation and respective cumulative permanent settlement. The numerical results were determined based on a 3D model that attempted to reproduce the experimental tests. The implemented permanent deformation model is described in the following expression:

$$\varepsilon_1^p(N) = \varepsilon_1^{p0}[1 - e^{-BN}]\left(\frac{\sqrt{{p_{am}}^2 + {q_{am}}^2}}{p_a}\right)^a \cdot \frac{1}{m\left(1 + \frac{p_{ini}}{p_{am}}\right) + \frac{s}{p_{am}} - \frac{(q_{ini} + q_{am})}{p_{am}}} \tag{3.2}$$

where p_{am} and q_{am} are the amplitude of the mean stress and deviator stress for train loadings, m and s are defined by the yielding criterion $q=s + mp$; and p_{ini} and q_{ini} are the mean and deviator stress in the initial state of the material; B, a and ε_1^{po} correspond to the material constants. Thus, this model includes the influence of the yielding criterion, initial stress state, and the stress induced by the passage of the train (Ramos et al., 2020).

This methodology is based on the number of load cycles and also on the stress levels induced by the passage of the train on the geomaterials that constitute the track. In this process, each load cycle corresponds to the passage of one axle, which means that the passage of the whole *Alfa Pendular* is equivalent to 24 load cycles. During the simulation of the long-term behaviour of the ballastless track in a transition zone, the evolution of the permanent deformation and the resulting dynamic effects are analysed in detail. This simulation method is based on the work developed by Alves Ribeiro (2012). However, in this case, a 3D model was considered while in the original work, a 2D model was used to study the behaviour of the transition zones. The simulation method consists of an iterative process through the articulation between the software ANSYS and the software MATLAB, according to the flow chart represented in Figure 3.10. Thus, in the commercial software ANSYS, the numerical modelling of the vehicle and the track is performed, as well as all the processes related to pre and post-processing of the results. In MATLAB, the results of the dynamic analysis are imported, and, based on the stress results, the permanent deformation is obtained (through the implementation of the permanent deformation law(s)). This methodology allows for the prediction of railway track settlement based on the stresses from 3D modelling of the transition (short-term performance), and the permanent deformation from a calibrated empirical permanent deformation model (long-term performance).

Analysing Figure 3.10, after the performance of the dynamic analysis, the stresses are obtained (vertical, horizontal and shear) in all finite elements of the FPL and subgrade, which are the only materials considered to contribute to the permanent deformation. Next the principal stresses are determined in MATLAB, as well as the *p'* and *q* stresses, which are the main inputs of the permanent deformation model.

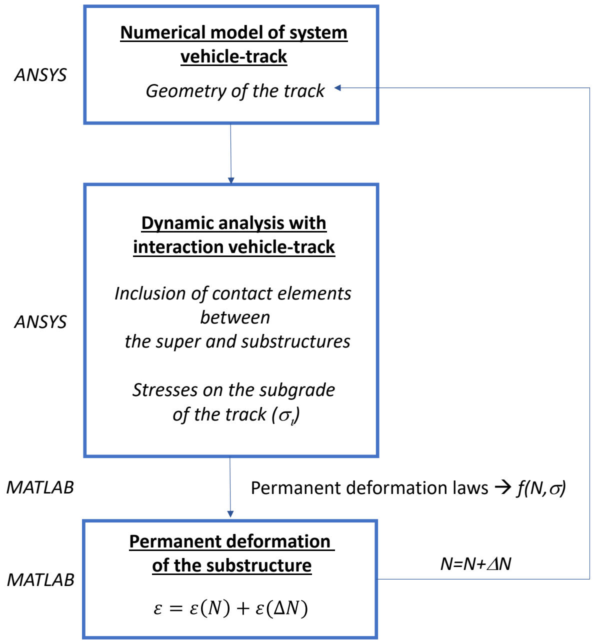

Figure 3.10 - Schematic representation of the simulation process of the permanent deformation of the track (adapted from Alves Ribeiro (2012))

The permanent deformation of the track induced by the passage of only one axle causes a very small deformation. This means that the process is not carried out cycle by cycle but in increments corresponding to a set of cycles (ΔN), assuming that, in this set of cycles, the stress state to which the materials are subjected remains constant. In this case, the selected ΔN adopted is 1 million cycles, which corresponds, approximately, to 1.5 years of West Coast Main Line (Kennedy et al., 2013) usage. This ΔN allows the development of the permanent deformation and its stabilisation (also known as plastic shakedown) (Werkmeister, 2003). After the determination of permanent deformation and permanent displacement in MATLAB, the results are read by the software ANSYS. Thus, ANSYS applies the permanent displacement to each node of the finite element, updating the geometry of the track.

After each dynamic analysis, the effects of the new geometry of the track on the dynamic behaviour of the transition zone can be evaluated. This procedure allows for the analysis of the joint effect on the variation of the stiffness and the settlement caused by the passage of the train after the passage of a certain number of axles.

3.2.1 Application of the methodology

The results regarding permanent deformation are presented considering absolute values. The number of cycles associated with each curve is 1 million cycles.

Considering the alignment under the loading, the results of the variation of the permanent deformation along the track are depicted in Figure 3.11 for the FPL and subgrade. In this case, the maximum permanent deformation for each vertical position was obtained, where y=0 m corresponds to the top of the rail. In the case of the FPL, there is an oscillation of the permanent deformation until the maximum (approximately x=-8m), followed by a decrease, an increase (approximately x=-4 m), and a sudden decrease until reaches the transition. Regarding the subgrade, there is a stabilization until x=-9 m, an increase (approximately x=-5 m), and a sudden decrease until the transition. These results are more obvious on the subgrade than the FPL since the permanent deformation and the stresses of the FPL are influenced by the contact elements placed at the top of this layer, which means that the analysis of the results is not as straightforward as in the subgrade. The analysis of Figure 3.11 c) also shows that the elements located from the middle of the subgrade layer only minimally contribute to the permanent deformation.

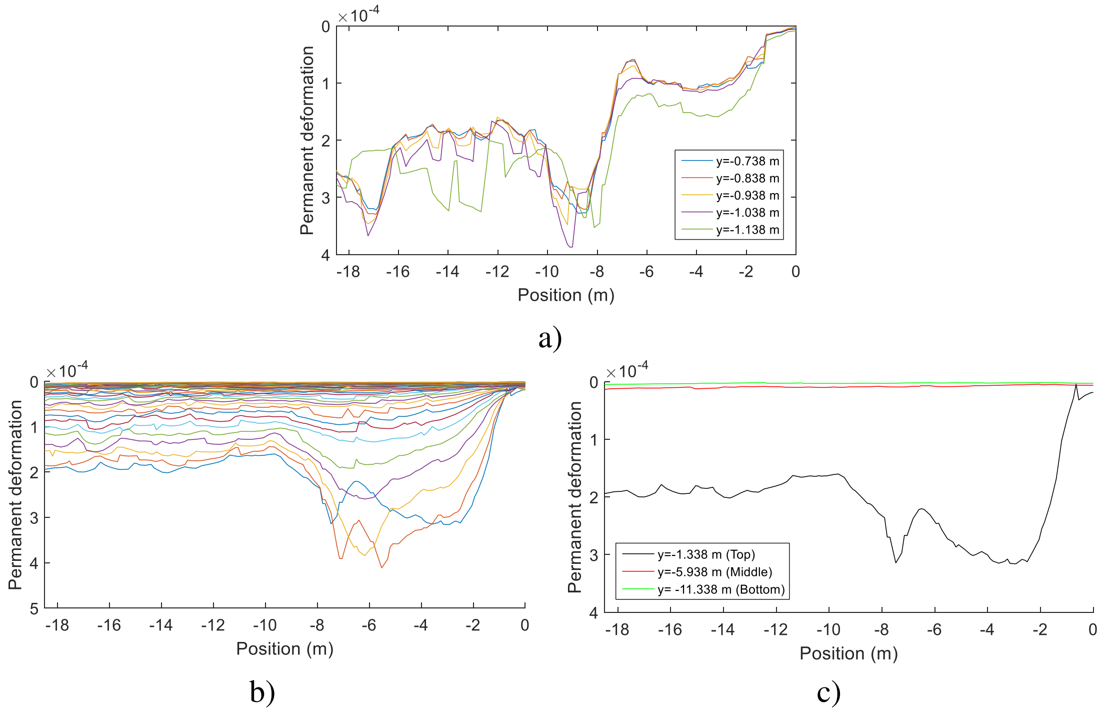

Figure 3.11 - Maximum permanent deformation a) of the FPL along the track (after 1 million cycles) for each vertical position; b) of the subgrade along the track (after 1 million cycles) for each vertical position; c) of the subgrade along the track (after 1 million cycles) for the top, middle and bottom nodes of the subgrade

Despite the importance of the previous results, it is also important to analyse cumulative permanent displacement:

$$\delta = \sum_{i=1}^{n} \varepsilon_{p_i} H_{si} \tag{3.3}$$

where i corresponds to the number of elements that constitute a certain material, H_{si} is the thickness of each element (in m), $\varepsilon_{p;i}$ is the permanent deformation at the centre of each element and δ is the cumulative permanent displacement of the track (in m).

This analysis was also performed considering the alignment under the loading. In Figure 3.12, the cumulative permanent displacements on the top nodes of the FPL and subgrade are presented. The maximum cumulative permanent displacement of the FPL in a range between 18.5 m<x<0 m occurs at x=-8.45 m. Regarding the subgrade, the maximum cumulative permanent displacement in a range between 18.5 m<x<0 m occurs at x=-7.15 m and corresponds to a value close to 0.46 mm, as depicted in Figure 3.12 b).

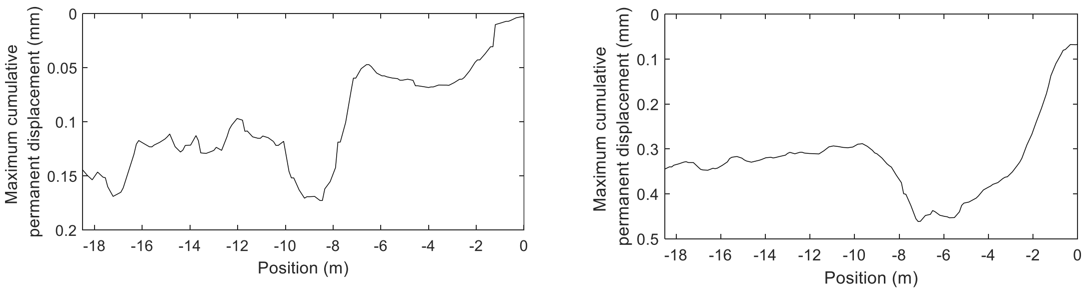

a) b)

Figure 3.12 - Cumulative permanent displacement in mm: a) on the FPL - variation of maximum cumulative permanent displacement along the track; b) on the subgrade - variation of maximum cumulative permanent displacement along the track

These results are important if analysed together considering the whole substructure with the inclusion of both layers: FPL and subgrade. Figure 3.13 shows the obtained results. The maximum cumulative permanent displacement of the substructure in the alignment under the loading is close to 0.52 mm in the range between -18.5 m <x<0 m and occurs at x=-7.25 m. The results depicted in Figure 3.13 a) also show that the layers that most contribute to the permanent deformation and respective cumulative permanent displacement are located between the top of the FPL (y=-0.738) and y=-4.138m (above half of the thickness of the subgrade). Indeed, all the layers of the FPL contribute to the development of the permanent deformation (and cumulative permanent displacement), as well as about 30% of the subgrade. After the depth y=-4.138m, the cumulative permanent displacement stabilises, which means that about 70% of the subgrade is not contributing to the development of the permanent deformation. This information is helpful since it shows that, in the design of the structure, special attention should be given to the properties of the subgrade above this depth (should be selected good quality materials).

Indeed, the value of 0.52 mm obtained in this numerical simulation is close to the value obtained in a full scale laboratory testing of a concrete slab where the maximum cumulative permanent displacement found was 0.53 mm (Čebašek et al., 2018). In this case, the structure was submitted to more than 3 million load cycles. Furthermore, in the work developed by Guo and Zhai (2018), the authors studied the long-term prediction of track geometry degradation (assuming a train speed of 300 km/h and a predicted time of 2 years, which corresponds to 350,400 million load cycles based on the actual daily traffic of about 60 trains with the 8 generalized train sets; the pre-set total passing number of the high-speed vehicles is thus $N\mathrm{t} = 8 \times 60 \times 365 \times 2 = 350400$) in high-speed vehicle-ballastless track system due to the differential subgrade settlement considering two different combinations of initial differential settlements of subgrade: 5mm/10 m and 5mm/20 m (co-sine functions). The accumulated subgrade settlement at different positions with respect to initial deformations show accumulated settlements below 1.5 mm and 0.9 mm considering the two combinations, respectively. Thus, it is possible to conclude that the obtained results are within this range of values.

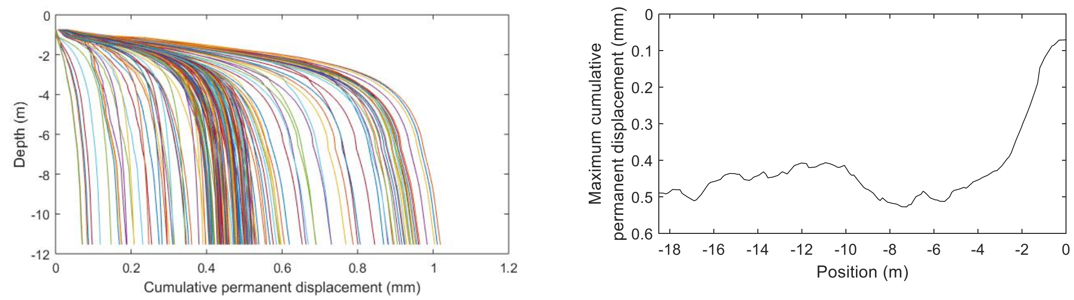

a) b)

Figure 3.13 - Cumulative permanent displacement on the substructure (FPL+subgrade) in mm: a) along the track (considering all the alignments); b) maximum cumulative permanent displacement along the track

The distribution of the cumulative permanent displacement (in mm) in the FPL and subgrade is presented in Figure 3.14. The colour scale shows the values of the cumulative permanent displacement in the bottom of FPL (Figure 3.14 a) and subgrade (Figure 3.14 b) along the x, y and z directions. Thus, in Figure 3.14 it is possible to conclude that the maximum cumulative permanent displacement may not occur exactly under the loading alignment. Furthermore, it is also possible to identify the peaks of the permanent deformation in all directions (Figure 2.5): vertical direction (y-axle), longitudinal direction (x-axle) and cross-direction (z-axle).

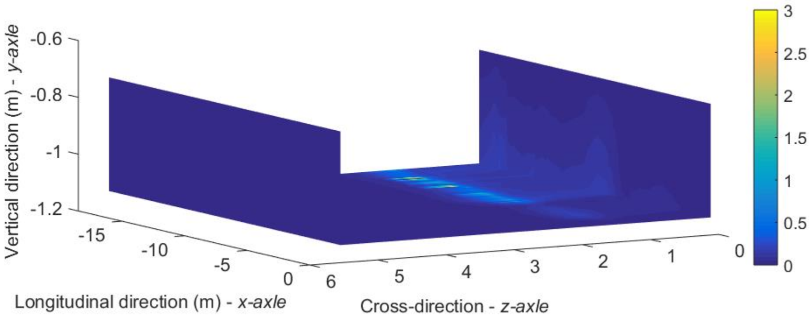

a)

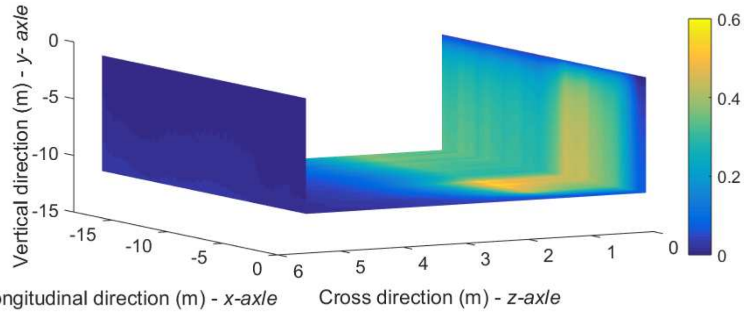

b)

Figure 3.14 - 3D cumulative permanent displacement in mm; a) on the FPL; b) on the subgrade

After the determination of the permanent deformation and permanent displacements (in meters), the obtained results were input to the 3D model (ANSYS) in each node of the FPL and subgrade.

3.2.2 Results of the dynamic analysis of the deformed track

The accumulation of permanent deformation with the number of load cycles can lead to a progressive change in the longitudinal profile of the track. Figure 3.15 shows the deformed profile along the longitudinal direction (*x*-axle) on the finite elements located at the top of the subgrade. The profile was scaled 500 hundred times to help to understand the impact that the deformed profile can have on the dynamic results.

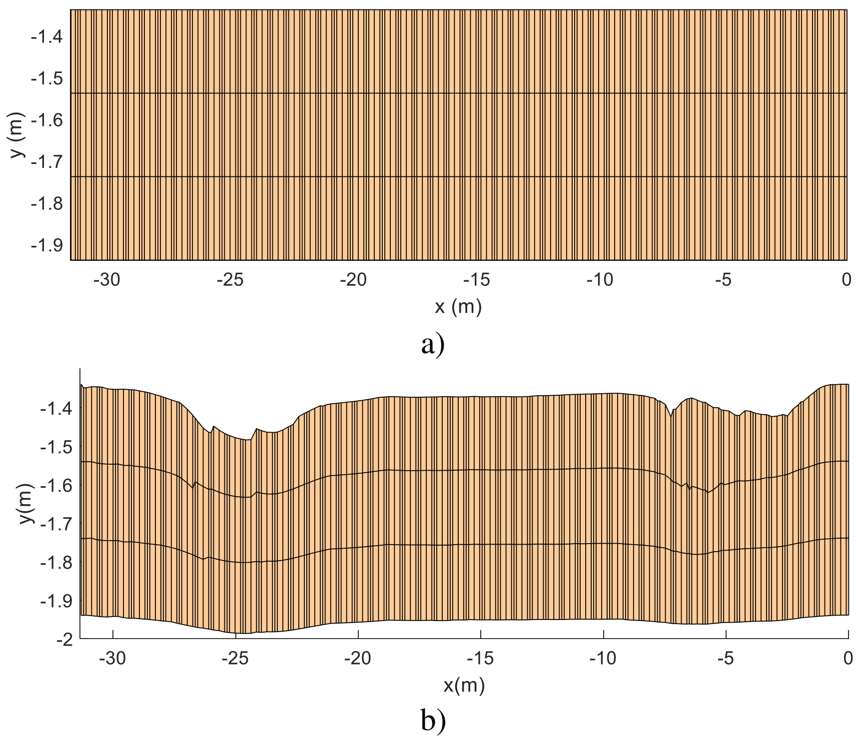

Figure 3.15 - Comparison between the original or non-deformed profile (a) and deformed profile (b) on the top of the subgrade – the deformation was augmented 500 times

Figure 3.16 presents the evolution of the vertical deformation along the track (including the transition zone in the case of the concrete slab and HBL) of the elements located on the top of the concrete slab, bottom of HBL and top of FPL and subgrade with the number of load cycles.

Analysing the results, it is possible to draw conclusions about the evolution of the permanent deformation on the track:

- The vertical deformation at the top of the concrete slab, bottom of HBL, top of FPL and top of the subgrade are similar;
- The impact of the evolution of permanent deformation is not significant. After 1 million cycles, the maximum increment in terms of vertical deformation is almost zero. The differences of the displacements between ΔN=0 and ΔN=1 million cycles along the track are almost impossible to identify.

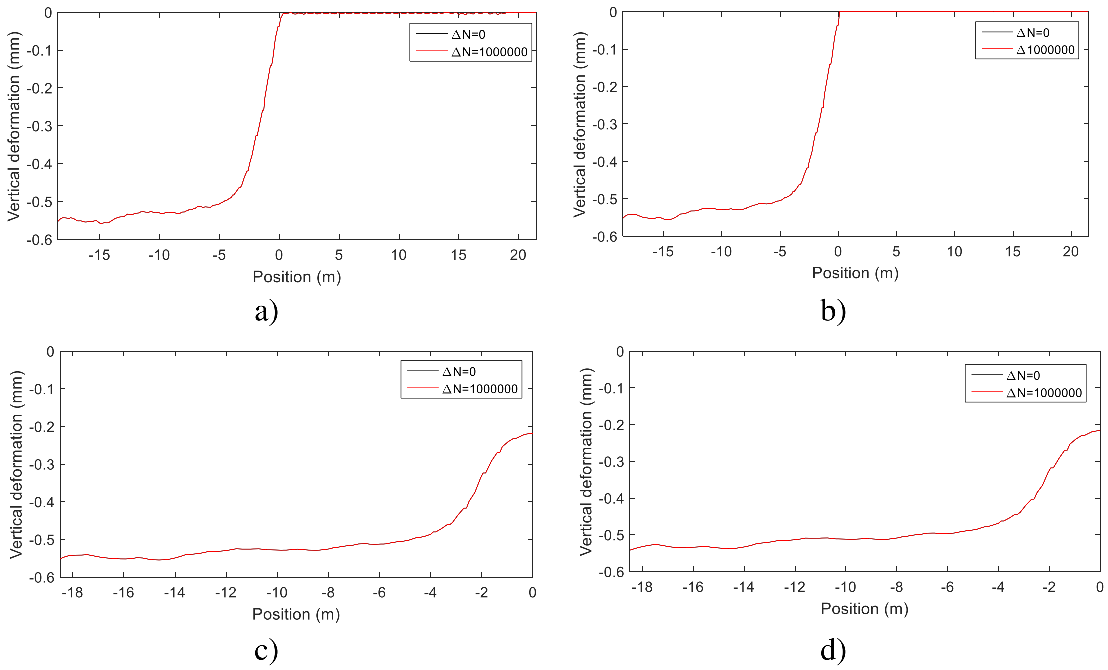

Figure 3.16 - Evolution of the vertical deformation along the track depending on the number of load cycles: a) top of the concrete slab under the loading alignment; b) bottom of HBL under the loading alignment; c) top of FPL under the loading alignment; d) top of the subgrade under the loading alignment

The variation of vertical stresses along the track on the top of the subgrade and FPL are presented in Figure 3.17. The results show a difference between the initial condition and the deformed track. However, the differences are not significant.

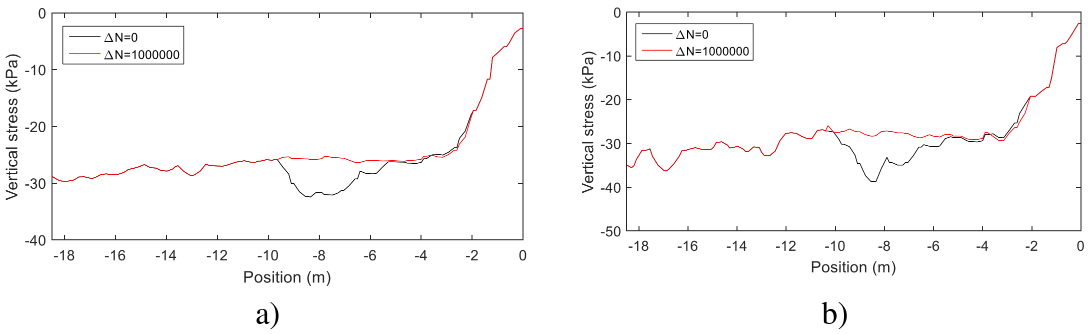

Figure 3.17 - Evolution of the vertical stress along the track depending on the number of load cycles: a) at the top of the subgrade under the loading alignment; b) at the top of the FPL under the loading alignment

The vertical displacement of the wheel over the deformed track includes the initial curve of the displacement induces by the train with the settlement profile of the substructure (the vehicle experiences total track deformation). However, the values of the permanent deformation are low due to the high stiffness of the track, which means that the settlement profile of the substructure is not so different when compared to the non-deformed profile. Indeed, as shown in Figure 3.13, the maximum cumulative permanent displacement of the substructure under the load alignment is less than 0.52 mm.

The variation of the vertical displacement of the wheel along the track with the number of load cycles is presented in Figure 3.18 a). The results show that there are no significant differences. In Figure 3.18 b) and Figure 3.18 c), the variation of wheel-rail interaction force and acceleration along the track with the number of load cycles are presented, respectively. However, as in the case of the displacements of the wheel, there are no major differences in the sections close to the transition zone. This is an indication of the good performance of the structure, which means that the increase in the number of cycles may have limited influence on the results regarding the short and long-term behaviour.

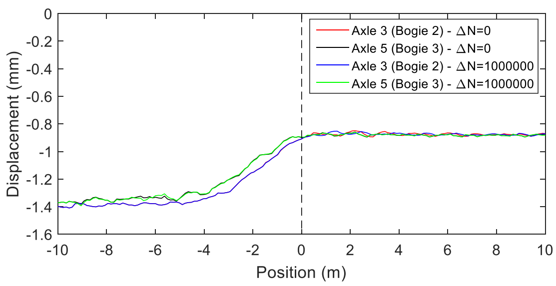

a)

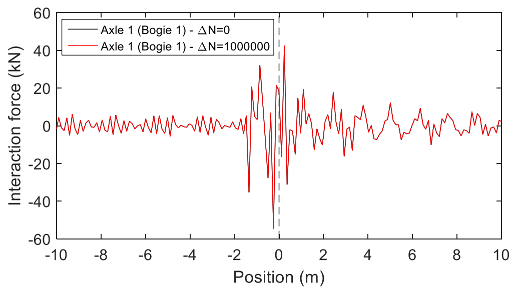

b)

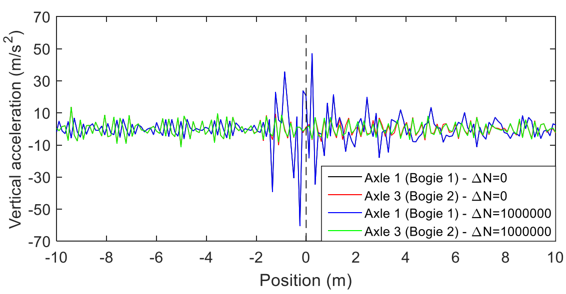

c)

Figure 3.18 - a) Dynamic vertical deformation of the wheel along the track with the number of load cycles: axle 3 and axle 5; b) variation of the interaction force wheel-rail of axle 1 along the track with the number of load cycles; c) variation of the acceleration of the axles along the track with the number of load cycles: axle 1 and axle 3

Figure 3.19 shows the maximum and minimum values of the vertical acceleration along the track at the bottom nodes of the HBL. Figure 3.20 a) shows the maximum values of the interaction force between the HBL and FPL in the alignment under the loading. In Figure 3.21, the variation of the maximum and minimum vertical and longitudinal stresses obtained along the transition zone at the top nodes of HBL with the number of load cycles are presented. The results show that the curves associated with the initial conditions (non-deformed track/ΔN=0) and the curve associated with a deformed track (ΔN=1 million load cycles) are overlaid in the transition zone (x=0m). This means that it is possible to continue the iterative procedure, incrementing the number of load cycles, to observe the increment of stresses and accelerations in this layer in the transition zone, as well as the interaction forces. Although, due to the good performance of the track, this increment of the number of load cycles may have a residual influence on these results.

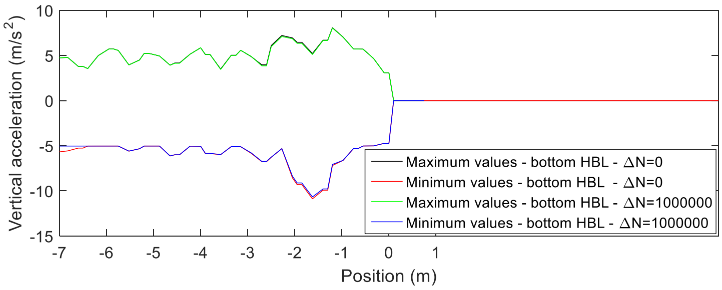

Figure 3.19 - Maximum and minimum values of the vertical acceleration of the HBL along the transition zone: bottom of the HBL under the loading alignment

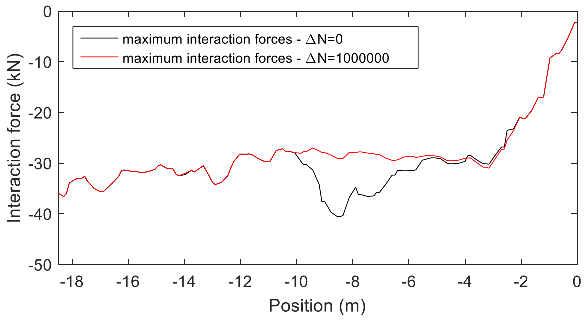

Figure 3.20 - Maximum Interaction force HBL-FPL along the track under the loading alignment

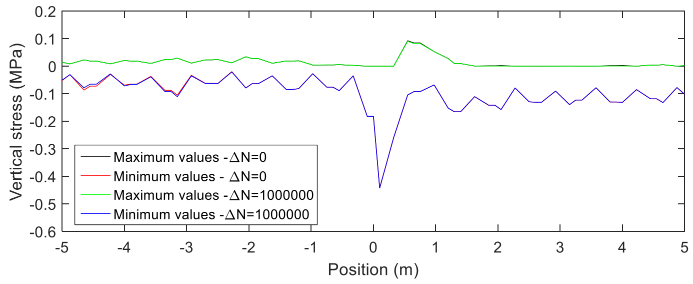

a)

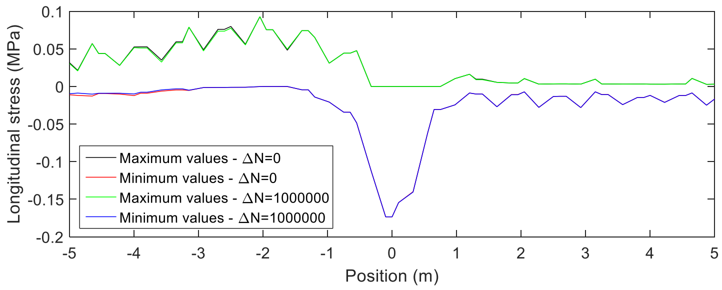

b)

Figure 3.21 - Variation stress in the top nodes of the HBL along the transition zone with the number of load cycles (under the loading alignment): a) vertical stress; b) longitudinal stress

From the previous results, it is possible to conclude that this specific transition zone with the ballastless track system shows a satisfactory performance after 1 million load cycles. The results show that the stiffness of the structure given by the concrete slab is significant when compared to the ballast used in the ballasted track. In this case, the long-term performance is only dependent on the subgrade and FPL that usually shows very low values of permanent deformation when compared to the ballast. Furthermore, in this study, the materials adopted in the FPL and subgrade present very good properties. However, the behaviour of alternative transitions may vary.

3.3 Improvement of the performance of the transition zone

Due to the concentration of the stresses on the concrete slab and HBL on the transition zone, a resilient mat was tested under the concrete slab in the tunnel and the embankment (1 m immediately before the transition) to try to mitigate this phenomenon, optimize the ballastless track and soft the transition, even despite the good long-term performance presented in the previous section. This mat, comprising a soft resilient layer, usually made from natural rubber because of its excellent dynamic properties, is important to give flexibility under the concrete slab and to balance the stiffness between the embankment and the tunnel. Furthermore, this can be an important step in the optimization of this system in transition zones.

Thus, considering the system presented previously, the original cement grout mass was replaced with a resilient mat in the tunnel zone (keeping the original 40 mm in order to not change the geometry of track), and also in the first meter of the embankment immediately before the transition, as depicted in Figure 3.22.

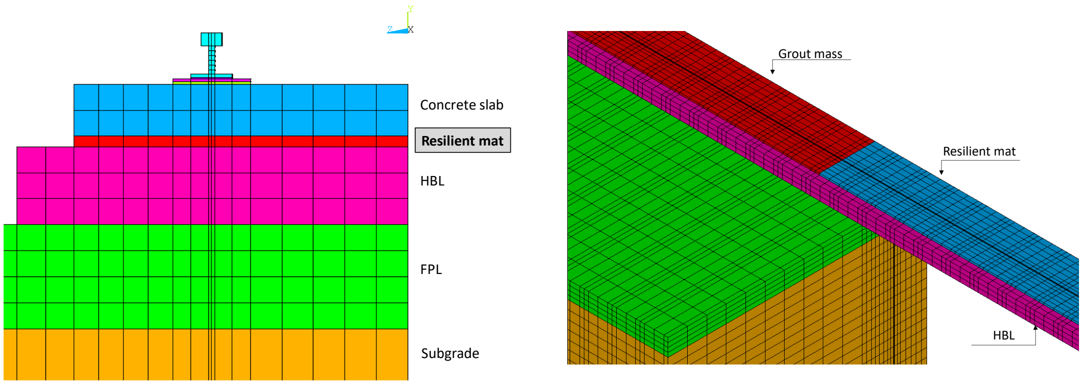

a) b)

Figure 3.22 - a) Position of the resilient mat; b) 3D model with the inclusion of the resilient mat in the transition zone

Taking into account this geometry, the resilient mat had a thickness of 40 mm and was modelled with solid elements. Several values of the stiffness of the resilient mat were tested in an iterative process. The adopted properties are shown in Table 3.2. The value of the dynamic stiffness (k) was adapted to obtain a smooth stiffness between the embankment and the tunnel with the resilient mat. The original value was obtained from the catalogue *Trackelast - Slab Track Mats* (Trackelast, -), along with the density. Regarding the damping, the values defined in the work developed by Zbiciak et al. (2017) were selected (ξ=2.5%). In this analysis, a *Poisson* ratio equal to 0 was adopted since the finite elements that are modelling the resilient mat are confined due to the connection to the concrete slab and HBL. This means that this material can only deform in the vertical direction.

Table 3.2 – Properties of the resilient mat

k (kN/mm^3)	**E (Pa)**	**ρ (kg/m3)**	**ν**	**α (ξ=2.5%)**	**β (ξ=2.5%)**
0.126	5.04×10^6	450	0	1.5325	3.88183×10^{-5}

k=stiffness; E = *Young* modulus; ρ = mass density; ν = *Poisson*'s ratio; α= parameter of the damping Rayleigh matrix that multiplies the mass' matrix of the system; β=parameter of the damping Rayleigh matrix that multiplies the global stiffness's matrix

Considering the geometry and the adopted properties, the displacements on the top nodes of the concrete slab were obtained. The results are depicted in Figure 3.23 and show a smoother transition (red line – resilient mat) when compared to the situation without a resilient mat where the displacements are zero from the transition at x=0m.

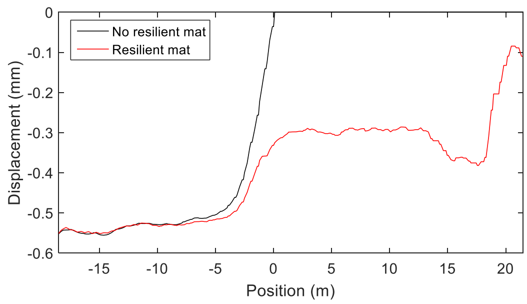

Figure 3.23 - Comparison of the displacements with and without resilient mat: maximum displacements on the top nodes of the concrete slab along the track

Despite the importance of the analysis of the displacements, it is imperative to evaluate the vertical and longitudinal stresses. The results regarding the concrete slab and HBL are presented in Figure 3.24.

The results depicted in Figure 3.24 show a reduction of the longitudinal and vertical stresses (σ_x and σ_y) along the track. Regarding the concrete slab, the results present a reduction of the maximum longitudinal stress value at x=0 m. Regarding the vertical stress, there is also a reduction of its value at x=0 m. This attenuation of the stress values is also visible in the HBL in terms of longitudinal and vertical stresses. Thus, despite the differences, the effects of the resilient mat are not extremely significant.

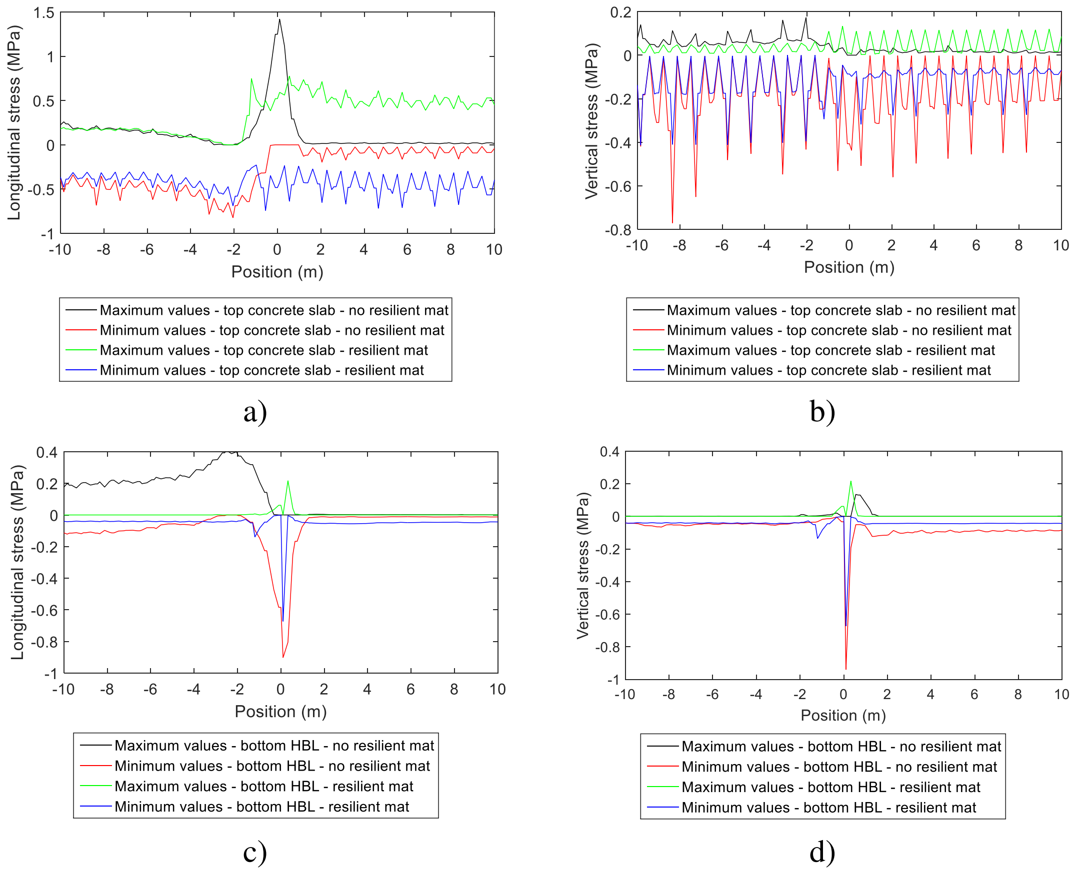

Figure 3.24 - Comparison of the stresses with and without resilient mat: a) longitudinal stresses along the track on the top nodes of the concrete slab; b) vertical stresses along the track on the top nodes of the concrete slab; c) longitudinal stresses along the track on the bottom nodes of the HBL; d) vertical stresses along the track on the bottom nodes of the HBL

4 Conclusions

This paper studies the performance of a ballastless track under varying support conditions across a transition zone. To do so, a 3D numerical model is developed and coupled with an empirical permanent deformation model to simulation of the degradation process of the track. Indeed, this modelling does not consider the important effect of water, which should be considered in future works. Moreover, the influence of the tunnel structure was not analysed in detail since this work is mainly focused on the stiffness transition and its long-term performance.

Regarding the short-term dynamic response of the track, the passage of four bogies is analysed in detail taking into account displacements, accelerations, and stresses in the ballastless track. The results show a high concentration of stresses in the concrete slab and HBL. Furthermore, the results show the variation of the vertical dynamic displacement of the axles and the increment of the vertical acceleration and wheel-rail interaction force at the transition zone centre. The displacements of the rails, concrete slab, HBL FPL and subgrade show a significant variation in response.

Regarding long-term behaviour, a hybrid methodology is implemented to simulate the settlement performance of the transition zone. To do so, the permanent deformation of the elements of the FPL and subgrade are calculated using MATLAB, based on the stress levels obtained from the 3D FE model. The settlement was is then posteriorly applied to the nodes of the 3D model. The results show that the maximum cumulative permanent displacement of the ballastless track over the embankment under the loading alignment is close to 0.52 mm. Furthermore, the structure shows satisfactory long-term performance after 1 million cycles. The iterative procedure with a higher number of load cycles should continue in future works. The results also show that only about 30% of the subgrade is contributing to the development of the permanent deformation and respective cumulative permanent displacement.

Due to the high concentration of stresses in the superstructure (concrete slab and HBL) at the transition zone, a resilient mat is included under the concrete slab in the tunnel and the first meter of the embankment immediately before the transition to try to mitigate this phenomenon. The mat gives additional flexibility to the system in the tunnel and reduces the higher stresses at the transition zone. In particular, the results show a reduction in the stress levels of the concrete slab and HBL.

Acknowledgments

This work was partially carried out under the framework of In2Track2, a research project of Shift2Rail. This work was also partly financed by FCT / MCTES through national funds (PIDDAC) under the R&D Unit Institute for Sustainability and Innovation in Structural Engineering (ISISE), under reference UIDB / 04029/2020. It has been also financially supported by national funds through FCT - Foundation for Science and Technology, under grant agreement [PD/BD/127814/2016] attributed to Ana Ramos. Additionally, it was financially supported by: Base Funding - UIDB/04708/2020 of the CONSTRUCT - Instituto de I&D em Estruturas e Construções - funded by national funds through the FCT/MCTES (PIDDAC). The authors also acknowledge the EU research project IN2ZONE.

References

Abdelkrim, M., Bonnet, G. & Buhan, P. D. 2003. A computational procedure for predicting the long term residual settlement of a platform induced by repeated traffic loading. *Computers and Geotechnics,* 30**,** 463–476.

Alves Ribeiro, C. 2012. *Transições Aterro – Estrutura em Linhas Ferroviárias de Alta Velocidade: Análise Experimental e Numérica.* PhD thesis Faculdade de Engenharia da Universidade do Porto, Porto, Portugal.

Alves Ribeiro, C., Calçada, R. & Delgado, R. 2018. Calibration and experimental validation of a dynamic model of the train-track system at a culvert transition zone. *Structure and Infrastructure Engineering,* 14**,** 604-618.

Alves Ribeiro, C., Paixão, A., Fortunato, E. & Calçada, R. 2015. Under sleeper pads in transition zones at railway underpasses: numerical modelling and experimental validation. *Structure and Infrastructure Engineering,* 11**,** 1432-1449.

Arema. Implementing track transition solutions for heavy axle load service. In Proceedings of the AREMA 2005 Annual Conferences, 2005 Chicago, IL, USA, 25–28 September 2005.

Asghari, K., Sotoudeh, S. & Zakeri, J.-A. 2021. Numerical evaluation of approach slab influence on transition zone behavior in high-speed railway track. *Transportation Geotechnics,* 28**,** 100519.

Banimahd, M., Woodward, P. K., Kennedy, J. & Medero, G. M. 2012. Behaviour of train-track interaction in stiffness transitions. *Proceedings of the Institution of Civil Engineers: Transport,* 165**,** 205-214.

Čebašek, T. M., A.F. Esen, Woodward, P. K., Laghrouche, O. & Connolly, D. P. 2018. Full scale laboratory testing of ballast and concrete slab tracks under phased cyclic loading. *Transportation Geotechnics,* 17**,** 33-40.

Chen, R., Chena, J., Zhaob, X., Bian, X. & Chen, Y. 2014. Cumulative settlement of track subgrade in high-speed railway under varying water levels. *International Journal of Rail Transportation,* 2**,** 205–220.

Coelho, B., Hölscher, P., Priest, J., Powrie, W. & Barends, F. 2011. An assessment of transition zone performance. *Proceedings of the Institution of Mechanical Engineers, Part F: Journal of Rail and Rapid Transit,* 225**,** 129-139.

Connolly, D., Giannopoulos, A. & Forde, M. C. 2013. Numerical modelling of ground borne vibrations from high speed rail lines on embankments. *Soil Dynamics and Earthquake Engineering,* 46**,** 13-19.

Dahlberg, T. 2004. Railway track settlements - a literature review. The EU project SUPERTRACK. Linköping, Sweden.

Ferreira, P. 2010. *Modelling and prediction of the dynamic behaviour of railway infrastructures at very high speeds.* PhD Thesis, Instituto Superior Técnico, Lisboa, Portugal.

Ferreira, P. A. & López-Pita, A. 2013. Numerical modeling of high-speed train/track system to assess track vibrations and settlement prediction. *Journal of Transportation Engineering,* 139**,** 330-337.

Fröhling, R. D. 1997. *Deterioration of railway track due to dynamic vehicle loading and spatially varying track stiffness.* PhD thesis, University of Pretoria. Pretoria.

Fröhling, R. D., Scheffel, H. & Ebersöhn, W. 1996. The vertical dynamic response of a rail vehicle caused by track stiffness variations along the track. *Vehicle System Dynamics,* 25**,** 175-187.

Grossoni, I., Powrie, W., Zervos, A., Bezin, Y. & Le Pen, L. 2021. Modelling railway ballasted track settlement in vehicle-track interaction analysis. *Transportation Geotechnics,* 26**,** 100433.

Guo, Y. & Zhai, W. 2018. Long-term prediction of track geometry degradation in high-speed vehicle–ballastless track system due to differential subgrade settlement. *Soil Dynamics and Earthquake Engineering,* 113**,** 1-11.

Hunt, H. E. M. 1996. Track settlement adjacent to bridge abutments. Paper presented at the Vehicle-Infrastructure Interaction IV, San Diego, CA. *Paper presented at the Vehicle-Infrastructure Interaction IV, San Diego, CA.*

Hunt, H. E. M. 1997. Settlement of railway track near bridge abutments. *Proceedings of the Institution of Civil Engineers: Transport,* 123**,** 68-73.

Indraratna, B., Babar Sajjad, M., Ngo, T., Gomes Correia, A. & Kelly, R. 2019. Improved performance of ballasted tracks at transition zones: A review of experimental and modelling approaches. *Transportation Geotechnics,* 21.

Johnson, K. L. 1985. *Contact Mechanics,* Cambridge, Cambridge University Press.

Kennedy, J., Woodward, P. K., Medero, G. & Banimahd, M. 2013. Reducing railway track settlement using three-dimensional polyurethane polymer reinforcement of the ballast. *Construction and Building Materials,* 44**,** 615-625.

Li, S., Wei, L., Chen, X., He, Q. & Chen, A. 2021. Dynamic characteristics of subgrade-bridge transitions in heavy-haul railways under roller excitation. *Transportation Geotechnics,* 29**,** 100589.

Li, Z. G. & Wu, T. X. Vehicle/Track Impact Due to Passing the Transition between a Floating Slab and Ballasted Track. In: Schulte-Werning B. et al. (eds) Noise and Vibration Mitigation for Rail Transportation Systems. Notes on Numerical Fluid Mechanics and Multidisciplinary Design, vol 99. Springer, Berlin, Heidelberg, 2008.

López-Pita, A., Teixeira, P. F., Casas-Esplugas, C. & Ubalde, L. 2006. Deterioration in geometric track quality on high speed lines: the experience of the Madrid-Seville high speed line (1992-2002). *Transportation Research Board 85th Annual Meeting.* Washington DC, United States.

Lundqvist, A., Larsson, R. & Dahlberg, R. 2006. Influence of railway track stiffness variations on wheel/rail contact force. Workshop Track for high speed railways, Porto, Portugal.

Lysmer, J. & Kuhlemeyer, R. L. 1969. Finite Dynamic Model For Infinite Media. *Journal of the Engineering Mechanics Division,* 95**,** 859-878.

Momoya, Y., Takahashi, T. & Nakamura, T. 2016. A study on the deformation characteristics of ballasted track at structural transition zone by multi-actuator moving loading test apparatus. *Transportation Geotechnics,* 6**,** 123-134.

Nicks, J. 2009. *The bump at the end of the railway bridge.* PhD Thesis, Texas A&M University

Nielsen, J. C. O., Lundén, R., Johansson, A. & Vernersson, T. 2003. Train-Track Interaction and Mechanisms of Irregular Wear on Wheel and Rail Surfaces. *Vehicle System Dynamics,* 40**,** 3-54.

Paixão, A. 2014. *Transition Zones in railway tracks - an experimental and numerical study on the structural behaviour.* PhD Thesis, Faculdade de Engenharia da Universidade do Porto, Porto, Portugal.

Paixão, A., Fortunato, E. & Calçada, R. 2013. Design and Construction of Backfills for Railway track Transition Zones. *Proceedings of the Institution of Mechanical Engineers, Part F: Journal of Rail and Rapid Transit,* 229 58-70.

Paixão, A., Fortunato, E. & Calçada, R. 2016. A contribution for integrated analysis of railway track performance at transition zones and other discontinuities. *Construction and Building Materials,* 111**,** 699-709.

Ramos, A., Gomes Correia, A., Calçada, R., Alves Costa, P., Esen, A., Woodward, P. K., Connolly, D. P. & Laghrouche, O. 2021. Influence of track foundation on the performance of ballast and concrete slab tracks under cyclic loading: Physical modelling and numerical model calibration. *Construction and Building Materials,* 277**,** 122245.

Ramos, A., Gomes Correia, A., Indraratna, B., Ngo, T., Calçada, R. & Costa, P. A. 2020. Mechanistic-empirical permanent deformation models: Laboratory testing, modelling and ranking. *Transportation Geotechnics,* 23**,** 100326.

Sañudo, R., Dell'olio, L., Casado, J. A. & Diego, S. 2016. Track transition in railways: A review. Construction and Building Materials. *Construction and Building Materials,* 112**,** 140–157.

Shahraki, M., Warnakulasooriya, C. & Witt, K.-J. 2015. Numerical Study of Transition Zone Between Ballasted and Ballastless Railway Track. *Transportation Geotechnics,* 3**,** 58–67.

Shahraki, M. & Witt, K.-J. 2015. 3D Modeling of Transition Zone between Ballasted and Ballastless High-Speed Railway Track. *Journal of Traffic and Transportation Engineering* 3**,** 234-240.

Shan, Y., Albers, B. & A., S. S. 2013. Influence of different transition zones on the dynamic response of track–subgrade systems. *Computers and Geotechnics,* 48**,** 21-28.

Trackelast. -. *Slab Track Mats* [Online]. http://www.trackelast.com/slab-track-mats.html: Trackelast Available: http://www.trackelast.com/slab-track-mats.html [Accessed 2020].

Varandas, J. N., Hölscher, P. & Silva, M. A. 2013. Settlement of ballasted track under traffic loading: Application to transition zones. *Proceedings of the Institution of Mechanical Engineering, Part F: Journal of Rail and Rapid Transit*.

Varandas, J. N., Hölscher, P. & Silva, M. a. G. 2011. Dynamic behaviour of railway tracks on transitions zones. *Computers & Structures,* 89**,** 1468-1479.

Varandas, J. N., Hölscher, P. & Silva, M. a. G. 2016. Three-dimensional track-ballast interaction model for the study of a culvert transition. *Soil Dynamics and Earthquake Engineering,* 89**,** 116-127.

Wang, H. & Markine, V. 2018. Modelling of the long-term behaviour of transition zones: Prediction of track settlement. *Engineering Structures,* 156**,** 294-304.

Wang, H. & Markine, V. 2019. Dynamic behaviour of the track in transitions zones considering the differential settlement. *Journal of Sound and Vibration,* 459**,** 114863.

Werkmeister, S. 2003. *Permanent deformation behavior of unbound granular materials.* PhD Thesis, University of Technology, Dresden, Germany.

Woodward, P. K., Laghrouche, O., Mezher, S. B. & Connolly, D. P. Application of Coupled Train-Track Modelling of Critical Speeds for High-Speed Trains using Three-Dimensional Non-Linear Finite Elements. International Journal of Railway Technology, 2015. 1-35.

Yu, Z., Connolly, D. P., Woodward, P. K. & Laghrouche, O. 2019. Settlement behaviour of hybrid asphalt-ballast railway tracks. *Construction and Building Materials,* 208**,** 808-817.

Zbiciak, A., Kraśkiewicz, C., Oleksiewicz, W., Płudowska, M. & Lipko, C. 2017. Mechanical modelling and application of vibroacoustic isolators in railway tracks. *MATEC Web of Conferences,* 117**,** 00090.

Zhang, S., Zhang, W. & Jin, X. 2007. Dynamics of high speed wheel/rail system and its modelling. *Chinese Science Bulletin,* 52**,** 1566-1575.